OPTICAL INVESTIGATION OF THE HEAT TRANSFER FROM A ROTATING CYLINDER IN A CROSSFLOW

M A GSCHWENDTNER

University of Canterbury / New Zealand

mag@mech.canterbury.ac.nz

This work was carried out at the University of the Federal Armed Forces in Munich / Germany.

The heat transfer from a rotating cylinder in an air-crossflow was investigated by purely optical measuring techniques. Flow velocities were measured by a two-dimensional LDV both in the vicinity of the cylinder and in the boundary layer. A new optical device based on light-deflection in a temperature field was developed to examine local temperature gradients in the boundary layer of the rotating cylinder. Finally, a Michelson-interferometer was installed to produce real-time pictures of isothermal lines around the heated cylinder. The impact of rotation on flow patterns, boundary layer behaviour and heat transfer could be clearly identified. It appears that the velocity-ratio Ω acts like an independent parameter, in that flow patterns correspond to this dimensionless number. Furthermore, it seems that rotation dominates over crossflow, both fluid-dynamically and thermally above $\Omega = 2$.

Eckert number   *heat transfer*   *rotating cylinder*   *crossflow*
boundary layer   *flow separation*   *optical measuring technique*

Laser-Doppler-Velocimeter   *light-deflection*   *interferometer*

List of symbols

Ec Eckert number

n Rotational speed

Re_∞ Reynolds number related to the flow

Re_Ω Reynolds number related to rotation

T_∞ Main flow temperature

ΔT Temperature difference

u	Velocity component
v_∞	Main flow velocity
y	Coordinate
φ	Angle
Ω	Velocity-ratio
Ψ	Stream function

Introduction

The motivation to investigate the heat transfer from a rotating cylinder can be found in the essence of what this situation can be considered to represent. If we look at the basic configuration of the experiment, a hot, rotating body in an air-flow, and imagine the surface straightened out, the problem presents itself in an even more fundamental sense: A fluid flow along a heated wall, or alternatively, a moving heated wall in a fluid.

Rotating bodies exposed to a gas flow occur in many technical applications. In aerospace the knowledge of thermo-fluid-dynamic phenomena of spin-stabilised flying objects is of critical importance, since rotation has a decisive impact on the occurring forces and therefore on the flight-path of e.g. re-entry bodies. With additional heat transfer problems like the cooling of rolling-bearings and of commutators of electric motors, the degree of complexity of the interaction between rotation and flow increases considerably. Especially with the development of highly complicated aeroplane engines, the knowledge of the thermo-fluid-dynamic processes around the parts exposed to the gas-flow are of fundamental importance. Here, the thermally extremely stressed turbine blades can be reduced to the problem of a moving wall with heat transfer as a first approximation.

The experiments reported here were carried out in hindsight of an investigation of the Eckert-number-phenomenon, which will be presented in a separate paper [13]. The Eckert-number-phenomenon describes a reversal of heat transfer at high rotational Reynolds numbers, despite the fact that the wall temperature is still below ambient, i.e. flow temperature. In order to understand the complex

interactions involved in the heat transfer of a rotating body in a crossflow, the critical flow parameters like fluid velocities, temperatures and temperature gradients had to be investigated. Therefore, mainly optical measuring techniques were employed, allowing precise and contact-free measurements without disturbing the sensitive flow in the vicinity of the cylinder wall.

Previous work

Many investigations of non-rotating cylinders in crossflow exist, yet only a few with rotation involved and hardly any with rotation and heat transfer. Only a brief overview of the existing experimental work on rotating cylinders is given here.

The first investigations of rotating cylinders had their main focus on the Magnus force, a force perpendicular to the crossflow. Reid [1] published his results about lift- and drag-forces on rotating cylinders in 1924. One of his main parameters was the velocity-ratio Ω, which is defined as the ratio of circumferential speed to the main flow speed. Reid explained the changing forces with a change of the complete flow pattern and a shift of the stagnation points.

At about the same time, experiments on the forces experienced by rotating cylinders were carried out by Thom [2]. He also took various influences into consideration, such as blockage-ratio, geometry of the cylinder and surface properties. Thom assumed that a layer of air attaches to the surface, isolating the cylinder from the external flow [3]. He determined the velocity profile in the boundary layer with a Pitot-probe and noticed a decrease in thickness of the boundary layer with increasing rotational speed [4].

Prandtl´s investigations on the flow around a rotating cylinder were of great importance for the use of Flettner-rotors on ships [5]. Prandtl acknowledged that the friction forces occuring in a fluid cause the development of a velocity profile in the boundary layer. The fact that the superposition of a translatory and a circular flow, like a rotating cylinder in a crossflow, create a lift-force many times larger than a comparable airfoil, was explained by Prandtl by the differing relative velocities to the fluid on each side of the rotating cylinder.

Swanson [6] gives an overview of the existing investigations and discusses the results under various aspects. He suggests the introduction of the origin of the boundary layer rather than the stagnation point which, in contrast to the non-rotating cylinder, is not necessarily identical. Swanson notes that with increasing velocity-ratio Ω the front stagnation point moves against the rotational direction and, by definition as a point with zero velocity, can no longer be situated on the wall. In other words, it becomes a free stagnation point. The lift-force is a result of the pressure difference between the upstream moving side of the cylinder and the downstream moving side, which again is the result of the different relative velocities between wall and crossflow. Swanson explains that the lift-force no longer increases as much with rotational speed above a velocity-ratio $\Omega = 3$ by noting that above this ratio, any point on the cylinder wall has a higher relative velocity than the crossflow.

As indicated above, there are only a few investigations on heat transfer of rotating cylinders. Comparisons with horizontal cylinders, where free convection provides the crossflow are of great interest. Anderson and Saunders [7] allegedly were the first to investigate the heat transfer of a horizontal, rotating cylinder in free convection. They used titantetrachloride for flow-visualisation and noticed an increase in boundary layer thickness at the critical Reynolds number. Furthermore, a shift of the flow separation in rotational direction up to the critical speed could be observed. From then onwards, the flow along the circumference of the cylinder was completely turbulent.

Impressive interferometric pictures can be found in the work of Etemad [8], who also carried out experiments on heated, horizontally rotating cylinders. He observed a shift of the point of boundary layer separation from the wall in rotational direction, until it completely vanishes with increasing speed. From then on, the influence of rotation predominates over the buoyant forces and the heat transfer increases.

Dropkin and Carmi [9] extended their experiments on horizontal cylinders up to rotational Reynolds numbers of $Re_{\Omega} = 4.3 \times 10^5$. They observed three ranges of

heat transfer dependent on rotational speed. In the first range the heat transfer coefficient remained nearly constant, whereas in the second it was positively influenced both by free convection and rotation. In the third range, however, above Re_Ω = 15,000, the heat transfer was solely determined by rotation, that is by the turbulence within the boundary layer.

Kays and Bjorklund [10] also included forced convection in their experiments. According to their results, forced convection had a critical influence on the heat transfer at low rotational speeds. From a velocity-ratio of $\Omega \approx 2$, rotation began to dominate the heat transfer. This observation is of particular interest as, at this very ratio, the front and rear stagnation point coincide, according to potential theory, and start to separate from the cylinder wall. From then on a persistent boundary layer exists around the circumference of the cylinder without flow separation, where the heat transfer is only determined by rotation. This is exactly what Etemad observed in his interferometric experiments.

The cooling of commutators of electric motors was investigated by Yildiz [11]. He confirmed that the heat transfer is only determined by rotation at higher speeds; however, it could not be increased any more above a rotational Reynolds number of Re_Ω = 2.5 x 10^6.

A theoretical study on the interaction of the Nusselt, Reynolds and Eckert numbers was carried out by Geropp [12]. His main focus was on high rotational speeds where the Eckert number, the ratio of the specific kinetic energy of a particle on the wall to the specific enthalpy difference between wall and surrounding fluid, and thus the frictional heat created by dissipation gains influence. As a result of his analysis it becomes obvious that the temperature gradient at the wall changes its sign at an Eckert number of about $Ec \approx 1$. This confirms Yildiz´ observation that the heat transfer can not be increased above a certain point. Geropp´s theory even predicts an opposite heat flow above an Eckert number Ec = 1, a phenomenon which is reported in a separate paper [13].

Peller et al. [14] identified three ranges of velocity-ratios Ω where the heat transfer showed different characteristics. In the first range, $0 < \Omega < 0.5$, a steep

increase of the Nusselt-number takes place, which the authors explain by the transition from laminar to turbulent boundary layer. In the second range, $0.5 < \Omega < 2$, the heat transfer is still independent of rotation, whilst at larger Ωs the crossflow no longer has any influence. In other words, the rotating cylinder behaves like an isolated cylinder without crossflow.

Badr and Dennis [15] performed a theoretical investigation on the heat transfer of a rotating cylinder with low flow velocities. In order to explain the calculated decrease of heat transfer at high rotational speeds, they propose the theory that a layer of fluid particles in the vicinity of the wall rotates in conjunction with the cylinder and acts like insulation with high thermal resistance.

Oesterle [16] used different gases in his experiments to reach higher Reynolds numbers. His LDV-measurements in the boundary layer confirmed that no separation points at the wall could be observed any more, above a velocity ratio $\Omega > 2$.

Experimental apparatus

Basic configuration

Providing the three principal requirements of crossflow, rotation and heating was achieved with the apparatus shown in figure 1. The crossflow is provided in a closed wind-tunnel in which a constant fluid temperature is maintained by a heat exchanger [17]. Although the wind-tunnel is gas-proof up to a pressure of 2 bar, the experiments were only carried out in air at ambient pressure. In this set-up gas-velocities of 70 m/s could be achieved.

Figure 1

ROTATING CYLINDER

GLASS PLATE

TEST-SECTION

LUBRICATION AND COOLING

ASYNCHRONOUS MOTOR

MOUNTING FLANGE FOR HEATING TUBE
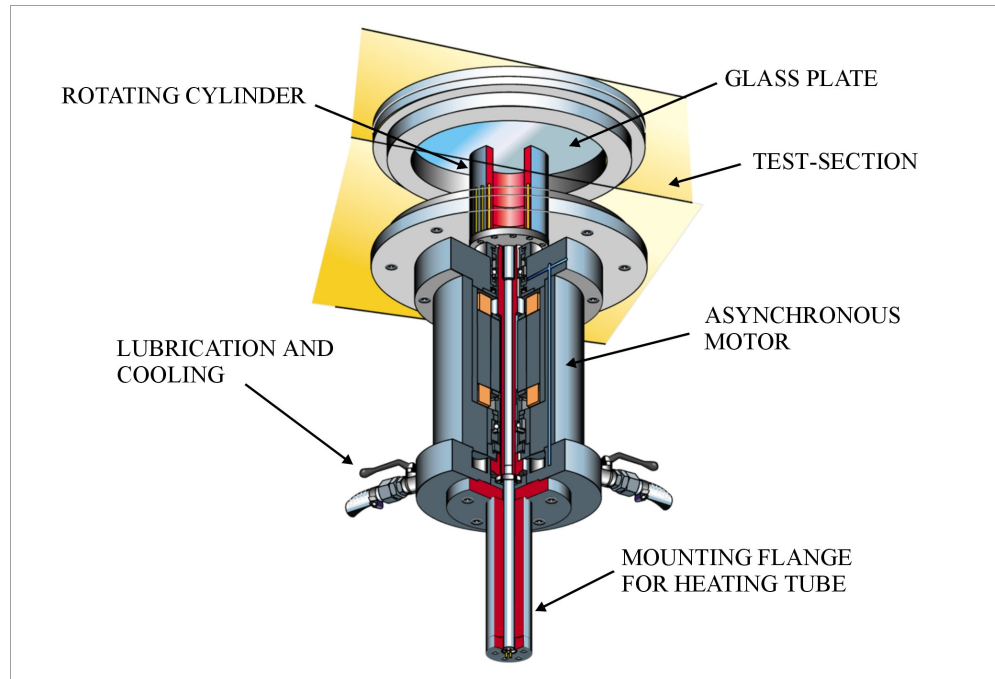
The rotating cylinder consists of high-strength aluminium and is mounted at the top of a hollow shaft of an asynchronous motor, which was designed for high-speed aluminium milling, and allowed rotational speeds up to 30,000 rpm (figure 1). This motor is attached to the bottom of the test-section, while the cylinder reaches vertically through the test-section.

The heat was supplied by a high performance heating cartridge which was mounted on a tube in the inner of the rotating cylinder. The tube was held by a flange at the bottom of the electric motor and led upwards through a hollow shaft. Thus, the heat was transferred from the non-rotating cartridge to the rotating cylinder by radiation only and the system worked reliably, regardless of the speed. However, the disadvantage was that the thermal inertia was relatively high and measurements could only be carried out after equilibrium had been reached.

A more detailed description of this set-up is given in a separate paper [13].

Measurement instrumentation

Overview

In order to examine the influence of rotation on the flow conditions in the surroundings of the cylinder a knowledge of the characteristic flow parameters is of great importance. Gas velocities were therefore measured with a two-dimensional Laser-Doppler-velocimeter (LDV) which is a highly complex optical measuring technique, but offers the advantage of accurate measurements without disturbing the sensitive flow. The driving force for heat transfer is temperature gradient. To determine the gradients, an optical measuring technique was developed, based on the deflection of a light beam in a temperature field according to Schmidt´s analysis [18]. Furthermore, the real-time observation of temperature fields in selected areas should allow insights into the actual processes around the cylinder. With a Michelson interferometer a third optical method was employed, with which the fluctuations of isothermals could be recorded on video.

Laser-Doppler-Velocimeter

A two-dimensional Laser-Doppler-Velocimeter (LDV) was employed to measure local gas velocities in the vicinity of the rotating cylinder. The principle of this measuring technique is based on the light-scattering of particles which are added to the flow, passing through an interference pattern created by two monochromatic light-beams. Just as the rattling noise of a stick on a fence is a measure for how fast someone walks, the velocity of the particle can be concluded from the frequency of the scattered light-pulses at a given width between the dark and light fringes of the interference pattern. (Note: It is not the shifted wavelength of the scattered light as the term "Doppler" falsely suggests!)

This complex optical measuring technique offers the advantage of quick measurements at high local resolution without disturbing the flow, as would be the case if hot wire probes, for example, were used. Also, data can be taken almost without delay, which allows dynamic measurements. Furthermore, in using two wavelengths of the laser, as in this case, two velocity components can be measured simultaneously at one position. Apart from that, this measuring

technique is independent of the pressure, temperature or density of the fluid. Figure 2 illustrates the main components of the LDV system.

Figure 2
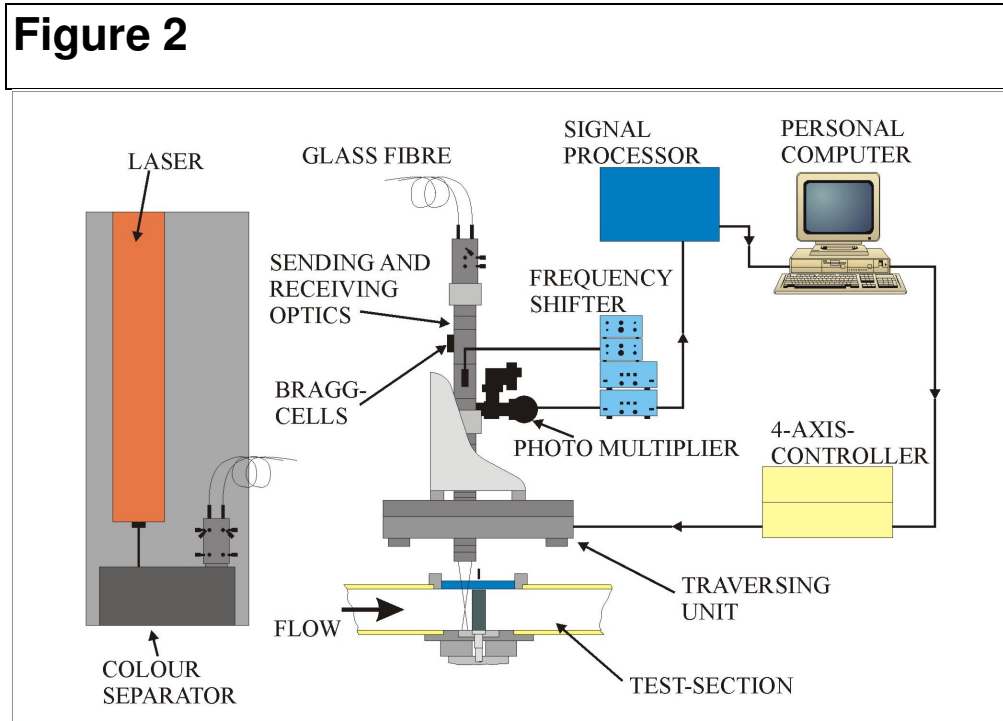
A 4 W Argon-Ion-Laser served as the light source for the LDV system. The laser operated in multiline-mode, which meant that all argon lines were emitted. A prism split the laser-beam into the respective colours, whereas two mirrors isolated the two most intensive wavelengths at 514.5 nm (green) and 488 nm (blue) for each velocity component. Both the laser and the colour separator were placed on a table which was damped against vibrations of the wind-tunnel.

The two colours were coupled into a glass-fibre which was connected to the sending and receiving optics above the test section. Here, each colour was split up into a pair, so that four parallel light beams passed through the sending and receiving optics. A front lens focused the beams to one point where the interference pattern was created and the measurement was taken. In order to detect the direction of each velocity component, one beam of each colour additionally passed through a Bragg-cell in which the light-frequency was shifted by 40 MHz. By intersecting with the second beam in the focal point, a moving interference pattern was created. Thus, a resting particle would exactly emit the shift-frequency of 40 MHz, whereas a moving particle would emit a higher or lower frequency depending on its direction relative to the shift direction.

The four beams passed through a highly precise glass plate which was let into the top of the test-section. Since the electric motor was attached at the bottom, the less efficient back-scattering mode had to be chosen. Thus, the scattered light was received by the same optical instrument, in which two sensitive photo multipliers detected the pulses of the scattered light of each colour respectively and converted them into electric pulses. A signal processor performed a Fourier-analysis and finally sent the data to a personal computer.

The sending and receiving optics were mounted on a 4-axis-traversing unit which was placed above the test section. Four highly accurate stepping motors allowed the positioning of the reading point to any arbitrary position around the rotating cylinder within an accuracy of ± 5 µm.

The size of the induced scattering-particles is of critical importance for the determination of the gas velocity. Larger particles produce scattered light of higher intensity; however, they do not necessarily represent the flow path of the gas molecules, due to their inertia. The opposite applies to smaller particles. Here, an aerosol was used which provided both a homogenous size distribution and good scattering properties. The aerosol was injected on the return of the wind-tunnel to the fan. Thus, an optimum mixing with the gas flow was guaranteed.

Light-beam deflection

Temperature gradients are the driving force for heat transfer, however, they can hardly be measured in a direct way, let alone contact-free. For this purpose an optical measuring technique was developed, which allowed the determination of local temperature gradients at the wall of the rotating cylinder without disturbing the sensitive boundary layer. The principle is based on E. Schmidt´s analysis [18] describing the path of parallel light near heated walls. According to this theory, light is being deflected in a density field towards higher density. With neglect of pressure differences the deflection of a light beam can be correlated with temperature gradients. Figure 3 depicts the experimental set-up.

Figure 3
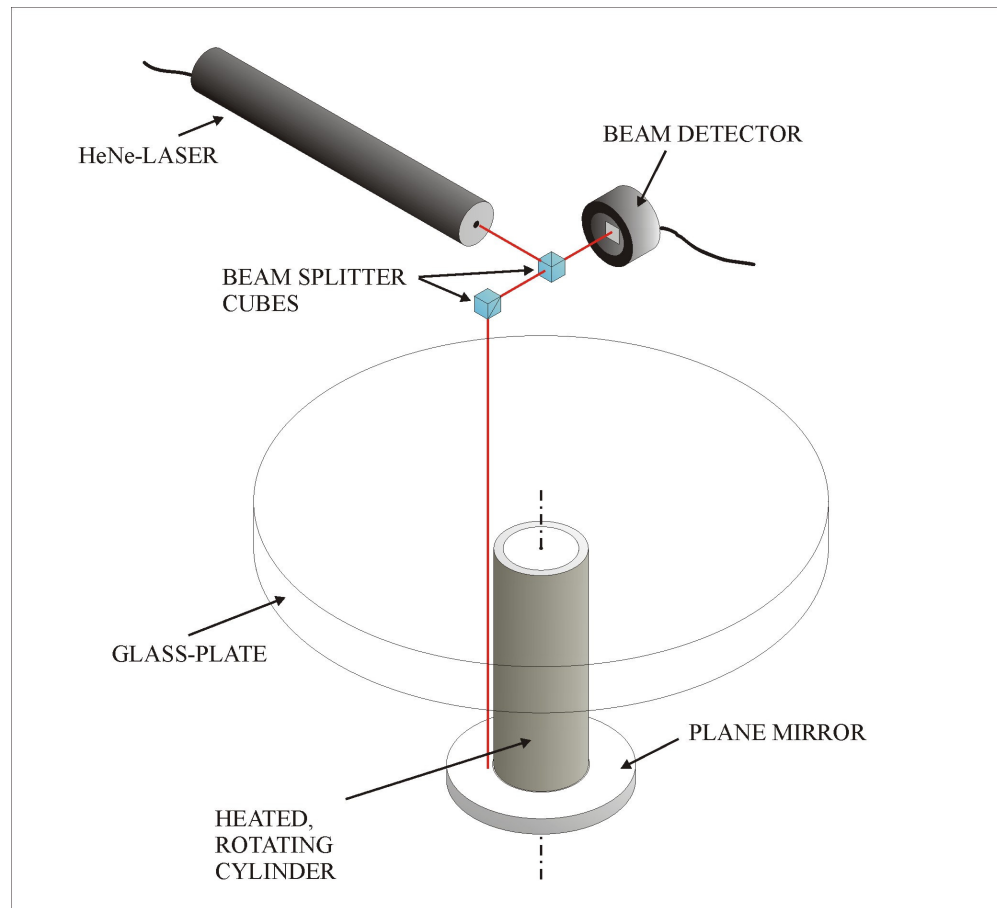
A light-beam coming from a small 5 mW helium-neon-laser is deflected by two beam splitter cubes so that it vertically enters the test-section through the optical glass-plate. The beam touches the cylinder wall, hits a mirror at the bottom of the test-section and is reflected back on itself. While passing through the beam splitter cubes again, one half of the remaining beam coming from the test-section hits a beam-position detector, which can measure the x,y-position of the centre of area with an accuracy of ± 50 µm. Laser, beam splitter cubes and detector, mounted together on a small plate, could be attached to the LDV-unit. Thus, the highly precise traversing unit could be used and the laser-beam could be positioned in polar-coordinates. However, this meant that the rotating axis of the traversing system, the optical axis and finally the rotating axis of the cylinder, all had to align. Eight degrees of freedom were available for this procedure. Unavoidable deviations were eliminated by a calibration procedure. Therefore, reference measurements were taken of an unheated cylinder before the actual experiments. The data was stored in a file which was used as an off-set for the subsequent measurements.

It should be noted that with this measuring technique, the final deflection of the light-beam is the result of an integration along twice the length of the cylinder. Deviations from two-dimensionality at both cylinder ends are therefore averaged. This means that a three-dimensional volume has to be regarded as the "reading point", which is formed by the height of the cylinder and the projection of the entering and departing light-beam. For instance, at a temperature difference of $\Delta T = 50\ K$ the deflection at the departure of the beam was about 1 mm. Also, the diameter of the light-beam of about 0.3 mm has to be accounted for. With respect to the radial extension of the "measuring point", the following cases have to be considered for the interpretation of the experimental results. Therefore, the range near the cylinder wall has to be subdivided into sections where the light beam can possibly travel. Figure 4 illustrates the qualitative deflection read by the detector over a radial shift of the light-beam.
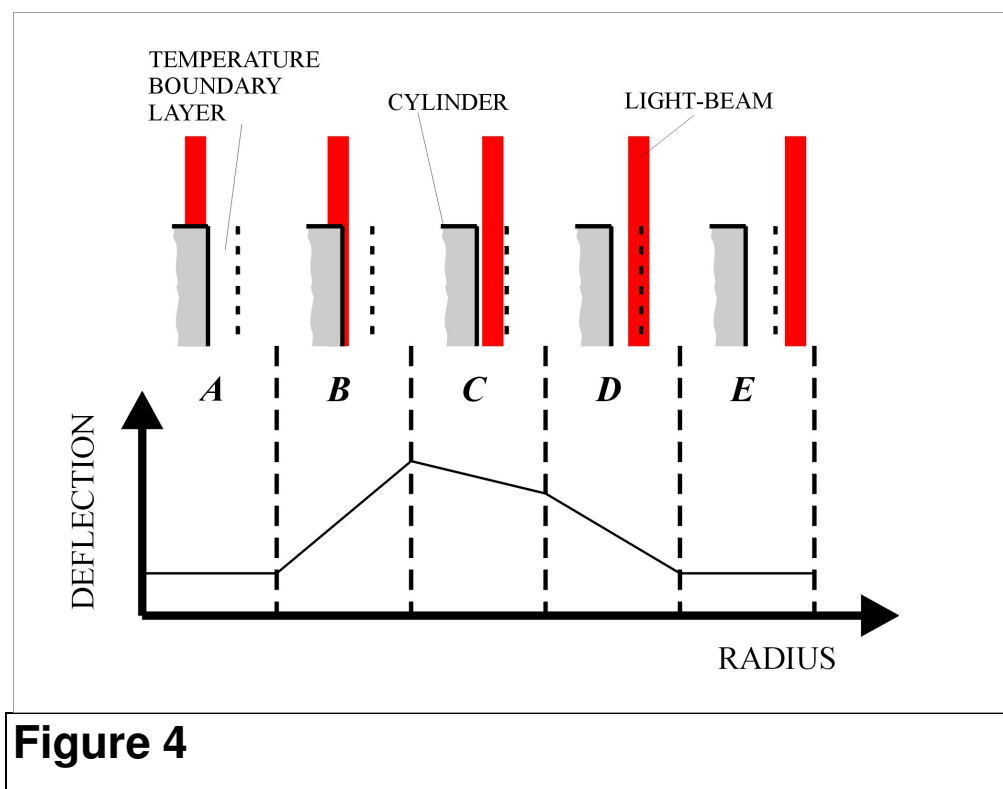
Figure 4

A: In the first section the complete light-beam hits the top of the cylinder. Hereby, the position of the light-spot does not change before reaching the border of the cylinder.

B: The first part of the light touches the cylinder wall and is reflected by the mirror. Due to the temperature profile in the boundary layer, the deflection is larger the closer the light-beam runs to the wall. Since the detector takes the centre of area of the light-spot, the deflection reaches a maximum once the light-beam fully hits the mirror.

C: The complete light-beam is now in the boundary layer now and travels to its border. Since the temperature gradient decreases towards the border of the boundary layer, the deflection also decreases.

D: In this section, the light-beam starts leaving the boundary layer. A faster decrease of the deflection takes place than in the previous section.

E: The complete light-beam is out of the boundary layer. There is no deflection any more.

Figure 5
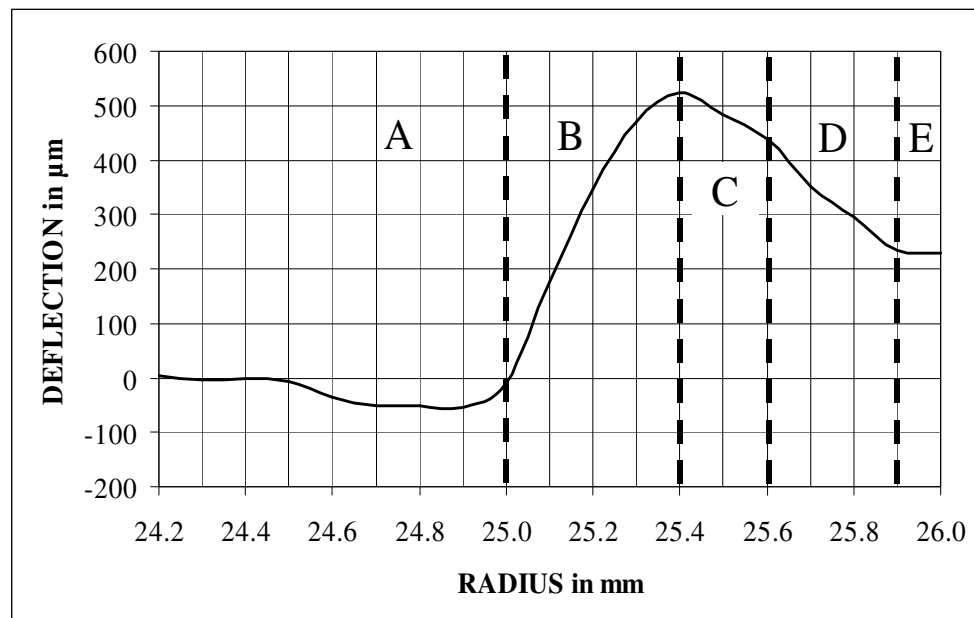
To illustrate this explanation of the light beam's behaviour, figure 5 shows experimental data of the light-deflection measured at the front-stagnation point of a non-rotating cylinder in an airflow at 10 m/s and a temperature difference of 50

13

K. The collected data confirm the previous considerations regarding the influence of the beam-diameter on the deflection.

At a cylinder radius of exactly 25 mm, the deflection of the light-beam starts (region B). The dip before can be explained by a reflection occurring at the top of the cylinder which has an annular, shiny surface there. The deflection peaks at a radius of 25.4 mm, then decreases (region C) and has a slight bend at 25.6 mm. From here on, the light-beam starts leaving the boundary layer (region D) and is completely out of this zone at 25.9 mm (region E). From this data it can be concluded that the beam has a diameter of about 0.3 to 0.4 mm and that the boundary layer ends on this stagnation point at the bend at a radius of 25.6 mm.

Michelson-interferometer

To visualize heat transfer processes and the impact of rotation in the vicinity of the cylinder, an interferometer was installed. The principle of this measuring technique is based on the superposition of two monochromatic and coherent light-beams which create a two-dimensional pattern of dark and light fringes. With the assumption that the gas obeys the laws of an ideal gas and that pressure differences change the density of the gas only marginally compared to temperature differences, interference fringes can be regarded as isothermals. The experimental set-up is shown in figure 6.

Figure 6
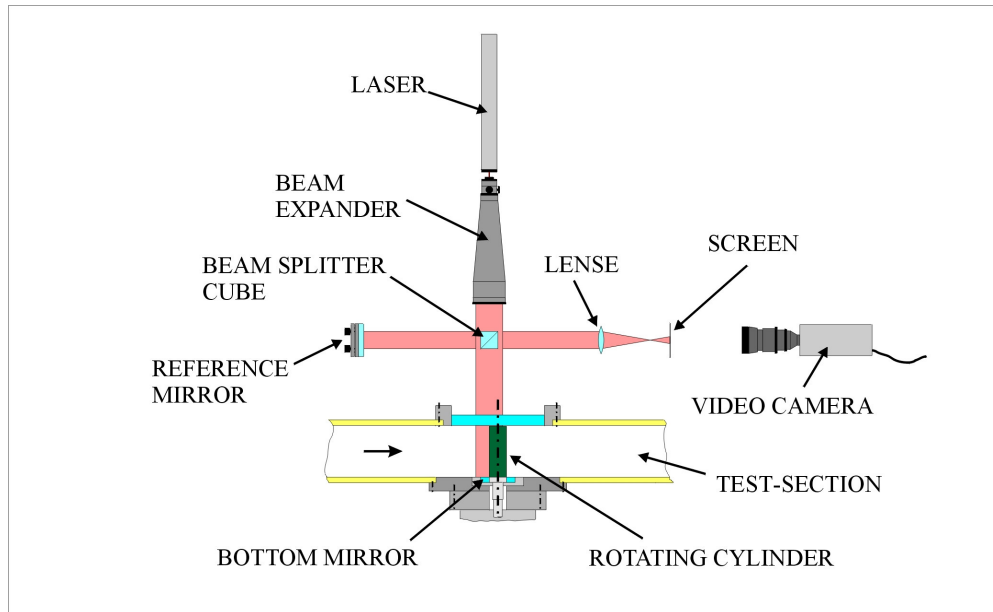
Light from a helium-neon-laser passes through a beam-expander which forms a plane wave-front of about 60 mm in diameter. A beam splitter cube splits the light in two equal parts, the reference and the measuring beam. The reference light is reflected by an adjustable plane mirror, passes the beam splitter cube again and is focused by a lens on a screen. The measuring beam enters the test-section, is reflected from the bottom mirror back to the beam splitter cube, where it superposes with the reference beam. While the reference beam remains unchanged, the wave front of the measuring beam is deformed by inhomogeneities of the light path, caused by either density or path-length differences. The result of the reunification of both light beams is partial amplification and extinction of light, depending on the local phase-difference.

The original intention to use the interferometer as an instrument for the qualitative determination of isothermals was quickly rejected. This was because the produced pictures did not allow the identification of isothermals, due to the extreme sensitivity of the optical set-up. (By means of a hot-wire-probe, the temperature difference between two interference fringes was determined to be approximately 0.05 K.) In other words, the density of the recorded fringes was beyond the optical resolution of the system. It was unavoidable that the interferometer was exposed to vibrations stemming from the wind-tunnel and the electric motor, as there was no possibility of separating the mechanical and the optical systems. Experiments to try to eliminate the fluctuations of the interference pattern by using extremely

short exposure times of only a few µs did not achieve the desired outcome. For all these reasons, the use of the interferometer was reduced to low gas velocities and small temperature differences, whereas the value of this measuring instrument mainly lay in the visualisation of the ongoing fluid-dynamic and thermal processes.

Experimental results

Fluid velocities

Outer field measurements

The purpose of the outer field measurements was to show the influence of rotation and heat transfer on the flow in the vicinity around the cylinder. Approximately 400 data points were taken on a grid with side lengths of 3 and 4 times the cylinder diameter. The chosen rotational speeds correspond to even numbers of the velocity ratio Ω. The temperature difference ΔT between the cylinder wall and the surrounding flow was 50 K, whereas the fluid temperature was maintained at 20 °C. The experiments were carried out mainly at sub-critical flow speeds, i.e. at Reynold numbers $Re_\infty = 3.3 \times 10^4$, which related to a main-flow velocity of 10 m/s corresponding to the cylinder diameter. However, for comparison, the experiments were extended to the critical Reynolds number of $Re_\infty = 1.1 \times 10^5$. The following figures 7 through 14 illustrate the flow around the cylinder in the unheated case, in sub-critical flow and velocity-ratios $\Omega = 0,1, 2$ and 3. In figures 7, 9, 11 and 13, the arrows represent the time-averaged, local velocity vector, according to magnitude and direction. The associated figure in each case (figures 8, 10, 12 and 14) shows the stream function which was calculated by numerical integration.

Figure 7

$v_\infty = 10$ m/s
$Re_\infty = 3.3 \times 10^4$
$T_\infty = 20\ ^\circ C$

$n = 0\ 000$ rpm
$Re_\Omega = 0$

$\Omega = 0$

$\Delta T = 0$ K

$v = 10$ m/s

Figure 8

$v_\infty = 10$ m/s
$Re_\infty = 3.3 \times 10^4$
$T_\infty = 20\ ^\circ C$

$n = 0\ 000$ rpm
$Re_\Omega = 0$

$\Omega = 0$

$\Delta T = 0$ K

STREAM FUNCTION:

$\Psi = \int u\, \partial y$
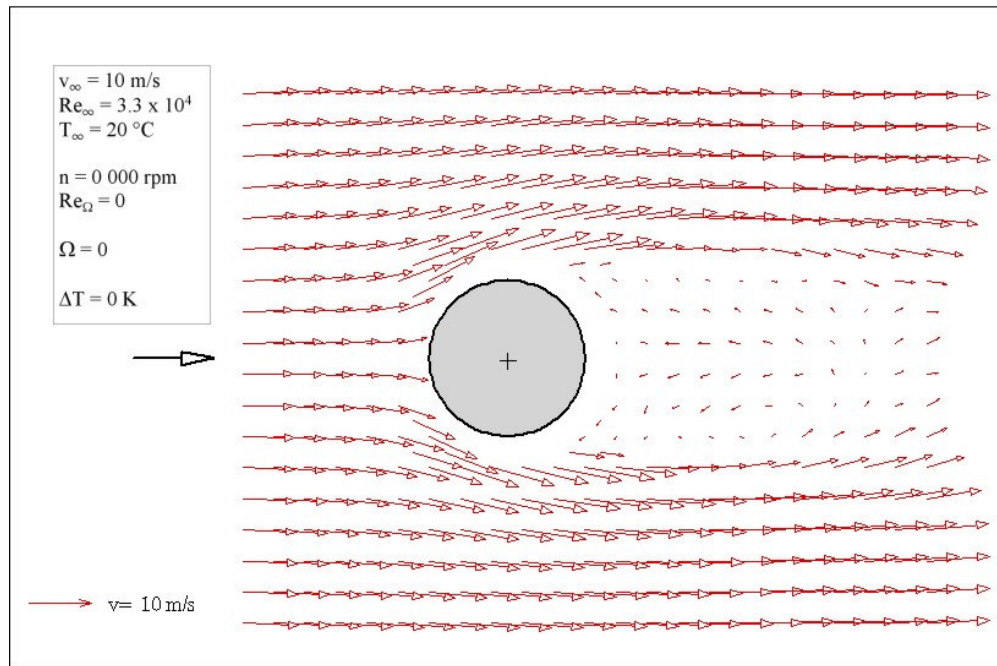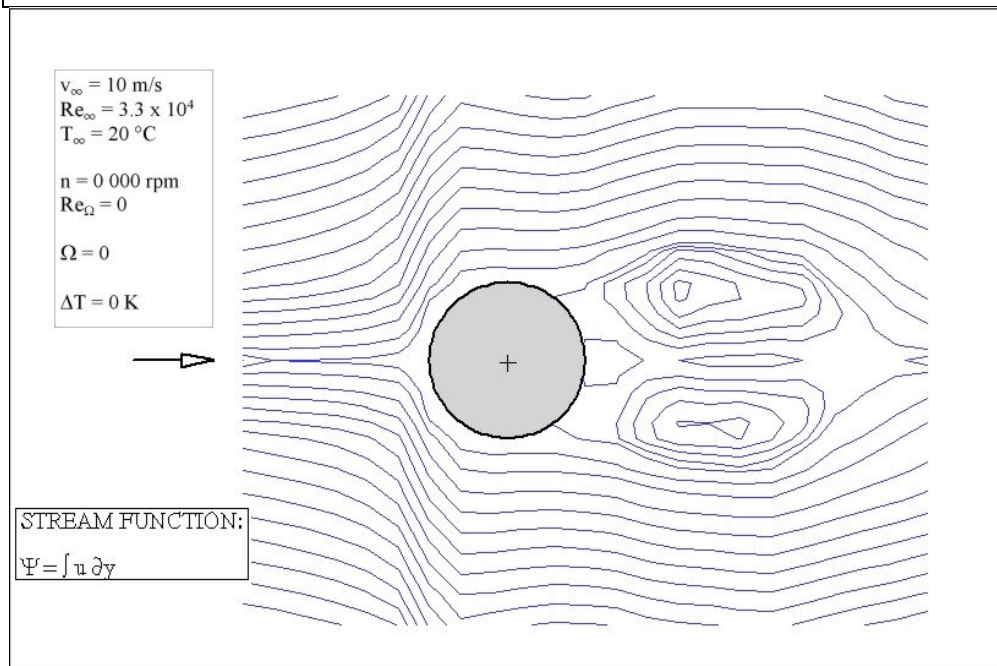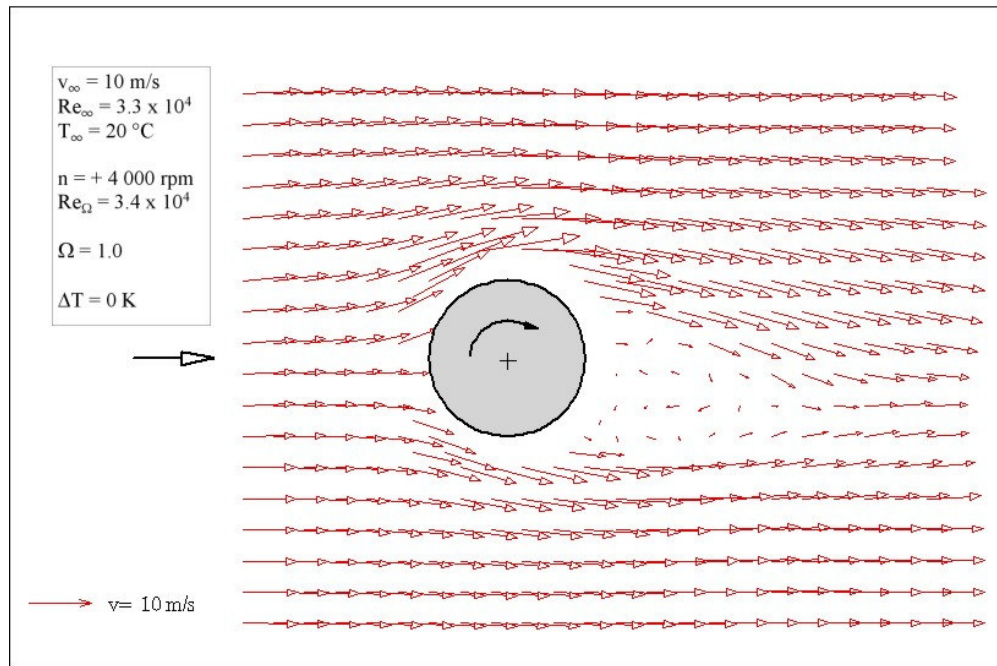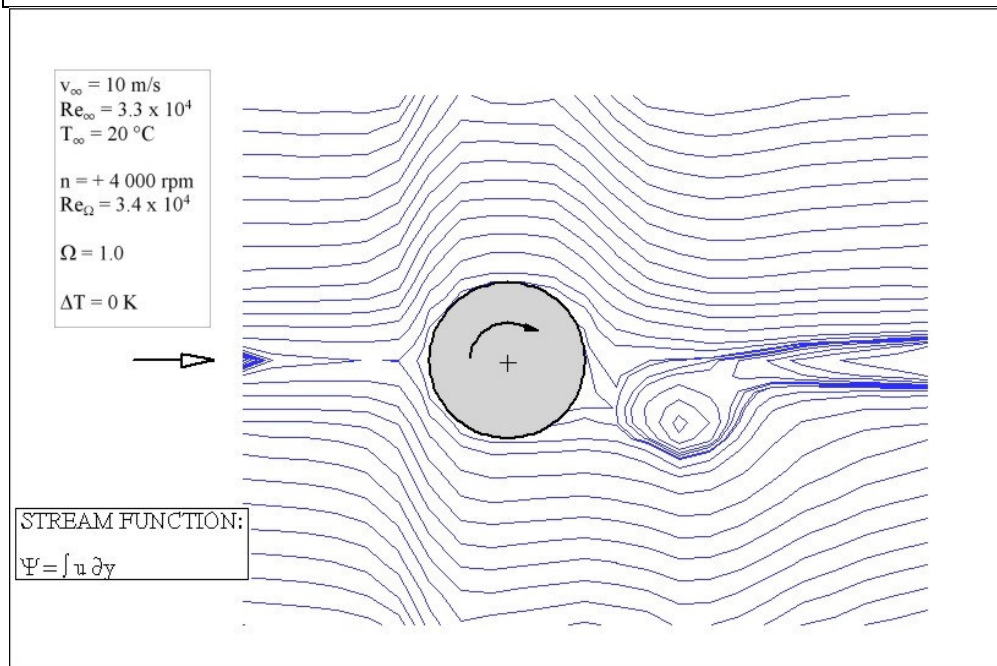
Figure 9

**Figure 10**

Figure 11

Figure 12

Figure 13

$v_\infty = 10$ m/s
$Re_\infty = 3.3 \times 10^4$
$T_\infty = 20\ °C$

$n = +\ 12\ 000$ rpm
$Re_\Omega = 1.0 \times 10^5$

$\Omega = 3.0$

$\Delta T = 0$ K

$v = 10$ m/s

Figure 14

$v_\infty = 10$ m/s
$Re_\infty = 3.3 \times 10^4$
$T_\infty = 20\ °C$

$n = +\ 12\ 000$ rpm
$Re_\Omega = 1.0 \times 10^5$

$\Omega = 3.0$

$\Delta T = 0$ K

STREAM FUNCTION:

$\Psi = \int u\, \partial y$
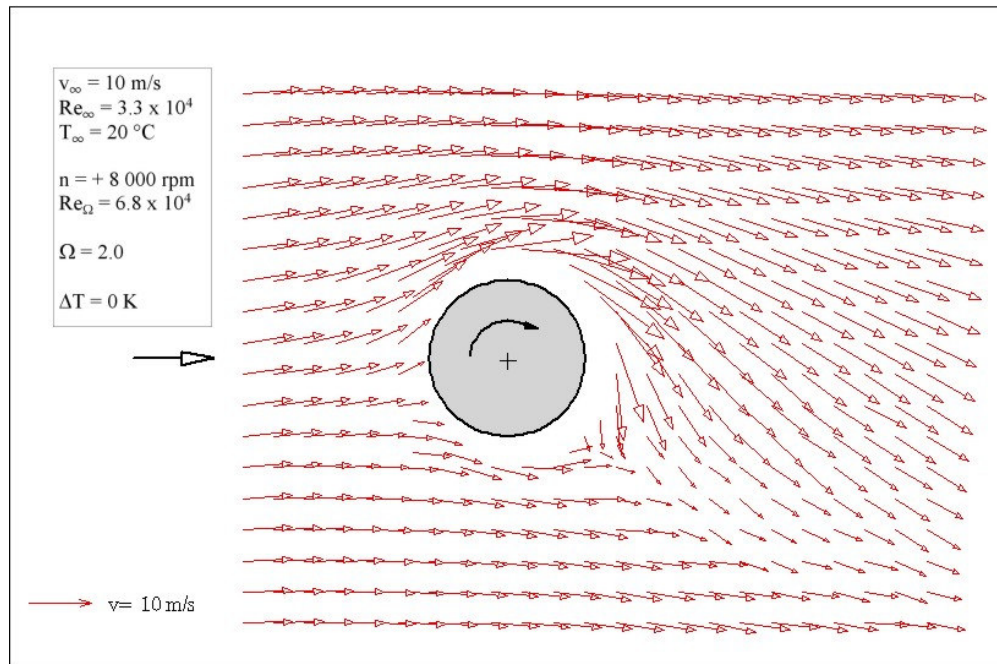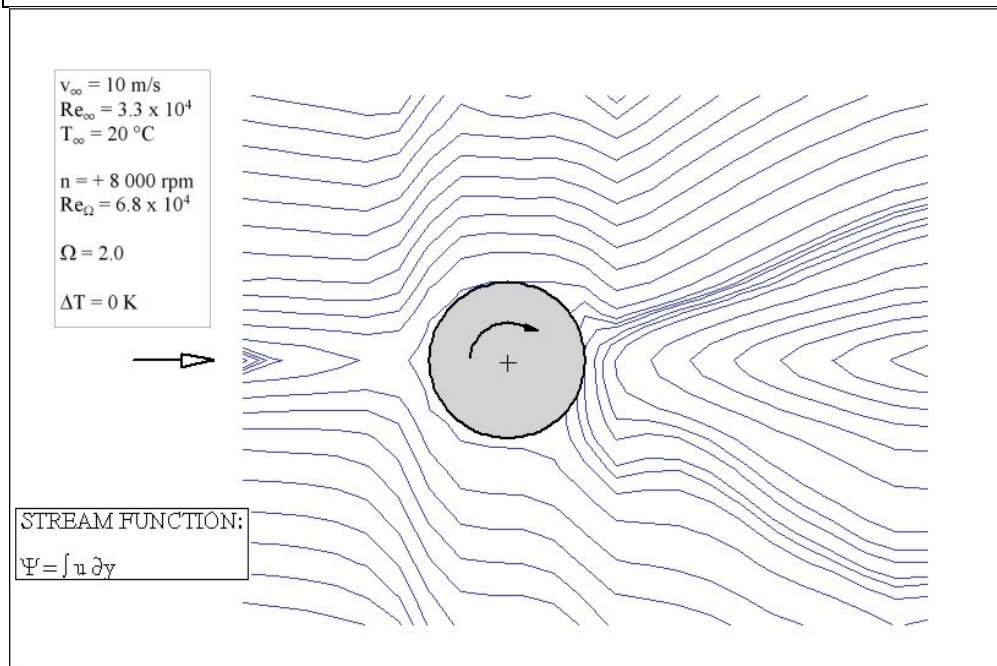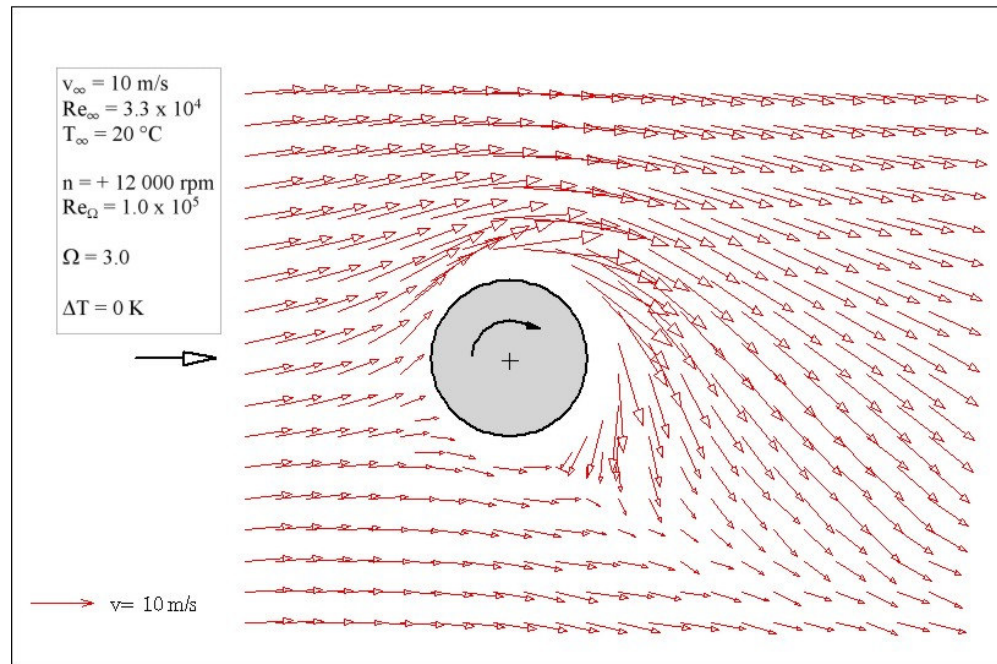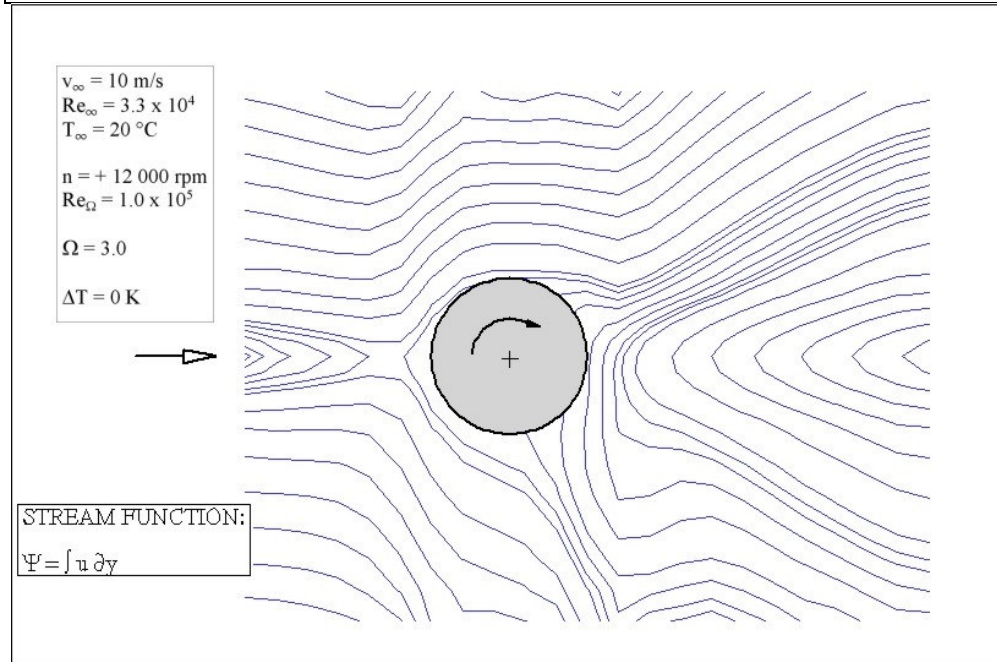
Figure 7 shows the case of the non-rotating cylinder. The flow is attached symmetrically to the cylinder and separates at an angle of about 90°. The wake is characterised by turbulence and re-circulation and stretches up to three times the cylinder diameter downstream. The streamlines in figure 8, calculated from the measured velocities, clearly show the typical twin-vortex structure in this area. With the onset of rotation (figure 9) the wake is asymmetrically deformed in the

rotational direction, with one separation point moving downstream and the other moving upstream. The twin-vortex structure is increasingly destroyed as the respective streamline picture (figure 10) illustrates. At a velocity-ratio of $\Omega = 2$ (figure 11) the turbulent wake is already significantly shifted. A further shift, however, cannot be observed at higher rotational speeds at $\Omega = 3$ (figure 13). This supports the already-mentioned observation by other authors that both separation points coincide at a velocity-ratio $\Omega = 2$ and that their position remains unchanged with increased speed. In the corresponding streamline pictures (figures 12 and 14) no vortices can be found any more, which indicates that there is no longer separation of the boundary layer at the cylinder wall. Thus, above $\Omega = 2$, a similar flow situation exists near the cylinder wall as in the case of a rotating cylinder without crossflow.

A significant change happens to the wake of the cylinder, however, when rotation is present. Figures 15 and 16 show the degree of turbulence in sections perpendicular to the main flow for non-rotating and rotating cases respectively.

Figure 15

$v_\infty = 10$ m/s
$Re_\infty = 3.3 \times 10^4$
$T_\infty = 20\ °C$

$n = 0\ 000$ rpm
$Re_\Omega = 0$

$\Omega = 0$

$\Delta T = 0$ K

DEGREE OF TURBULENCE --->

Figure 16

$v_\infty = 10$ m/s
$Re_\infty = 3.3 \times 10^4$
$T_\infty = 20\ °C$

$n = +\ 4\ 000$ rpm
$Re_\Omega = 3.4 \times 10^4$

$\Omega = 1.0$

$\Delta T = 0$ K

DEGREE OF TURBULENCE --->
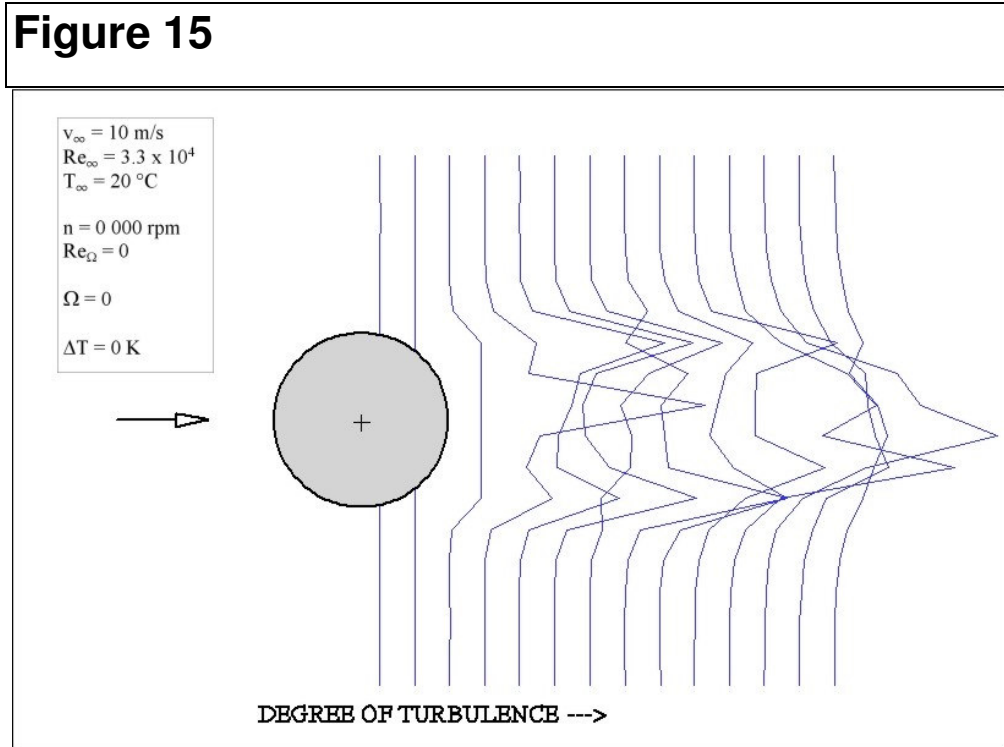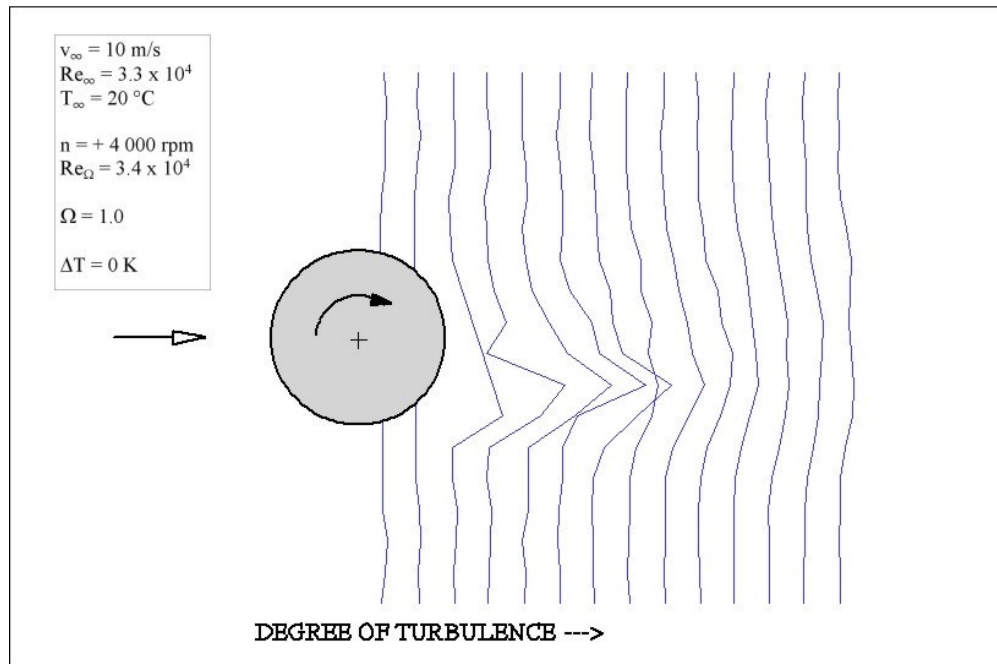
The complete wake is highly turbulent in the case of the non-rotating cylinder, and this is especially evident at the border to the main flow (figure 15). A reason for this may be the higher shear-forces in this particular flow area. Figure 16 demonstrates the effect of rotation on the extent of turbulence in the wake of the cylinder. The result is a significant reduction of turbulence, with the exception of the area in which the isolated vortex is located.

Figure 17

$v_\infty = 20$ m/s
$Re_\infty = 6.6 \times 10^4$
$T_\infty = 20\ °C$

$n = +\ 8\ 000$ rpm
$Re_\Omega = 6.8 \times 10^4$

$\Omega = 1.0$

$\Delta T = 0$ K

v= 10 m/s
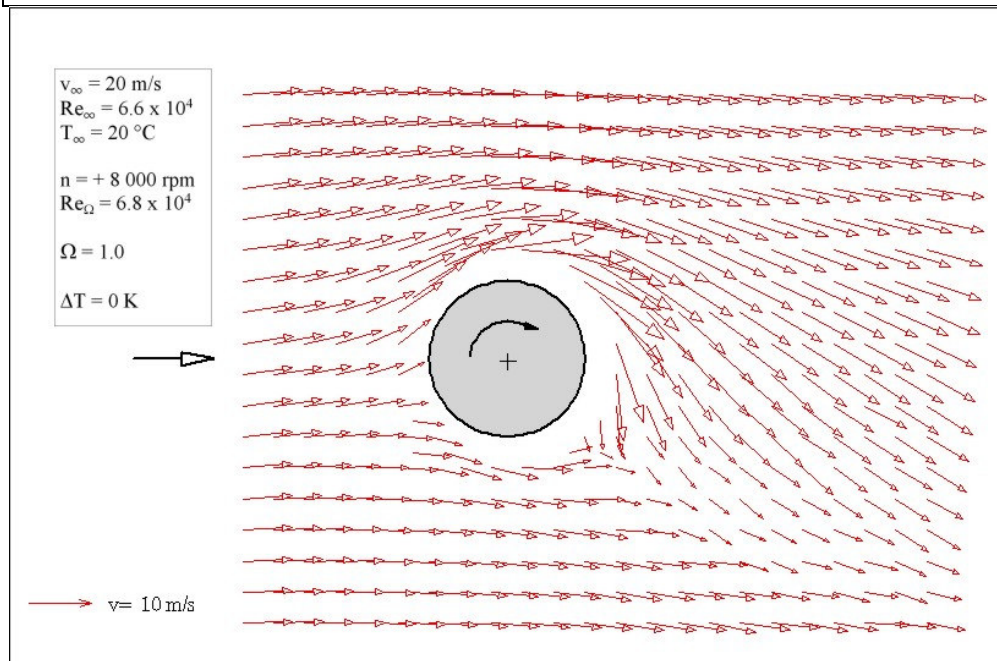
An increase of the flow velocity up to the critical range has no effect on the flow pattern, as figure 17 illustrates. Here, the Reynolds number is about twice as high as in the sub-critical case in figure 9, with a velocity-ratio $\Omega = 1$ in both experiments. A comparison of both pictures does not indicate any obvious differences.

Furthermore, heat rejection has no significant influence on the flow characteristic in the surroundings of the cylinder as the following experiments demonstrate. Figure 18 depicts the non-rotating cylinder in sub-critical flow with the cylinder surface heated to 50 K above the fluid temperature (i.e. $\Delta T = 50$ K). Also shown in figure 19 is the heated case ($\Delta T = 50$ K) for a velocity-ratio $\Omega = 2$. No significant differences can be seen between these two figures and the corresponding unheated cases (figures 7 and 11 respectively).

Boundary layer measurements

For the velocity measurements in the closest vicinity to the cylinder wall the traversing unit was moved in polar coordinates. The angular steps were 15°, and the radial movement was in the range from 0 to 4 mm with a step increment of 0.2 mm. Altogether, it was a measuring domain in which there were 480 reading points. The smaller fluid velocities in the boundary layer result in fewer scattering particles in this area, and thus a lower signal rate. For this reason only the tangential component of the velocity was measured with the more intense green light. This seems to be justified as Peller [19] proved that the deviation from the total velocity remains below 5 % with only the tangential component being measured in the boundary layer.

In the following figures 18 to 21 the radial coordinate is magnified by the factor four for clarity. These figures illustrate the case of sub-critical flow at different velocity-ratios Ω without heating. The small velocities at the back of the non-rotating cylinder (figure 18) indicate the turbulent wake. At an angle of about $\varphi = 90°$ the fluid has already clearly separated from the wall. With some rotation present ($\Omega = 1$, figure 19) a significant increase in velocity of the fluid can be

observed on the downstream side of the cylinder. Although a layer of particles (at least 0.4 mm thick) attached to the rotating wall has already formed around the complete circumference of the cylinder, a noticeable change in flow direction in the boundary layer occurs at an angle $\varphi = 270°$. With increasing rotational speed at $\Omega = 2$ and 3 (figures 20 and 21) more and more particles are carried away by the rotating wall so that the layer which is resting relative to the wall increases in thickness. The apparent changes in direction of the fluid velocities in the back of the cylinder on the downstream side can be explained by a too small number of signals due to the lack of scattering particles in this zone and are therefore false.

Figure 18

$v_\infty = 10$ m/s
$Re_\infty = 3.3 \times 10^4$
$T_\infty = 20$ °C

n = 0 000 rpm
$Re_\Omega = 0$

$\Omega = 0$

$\Delta T = 0$ K

v= 10 m/s
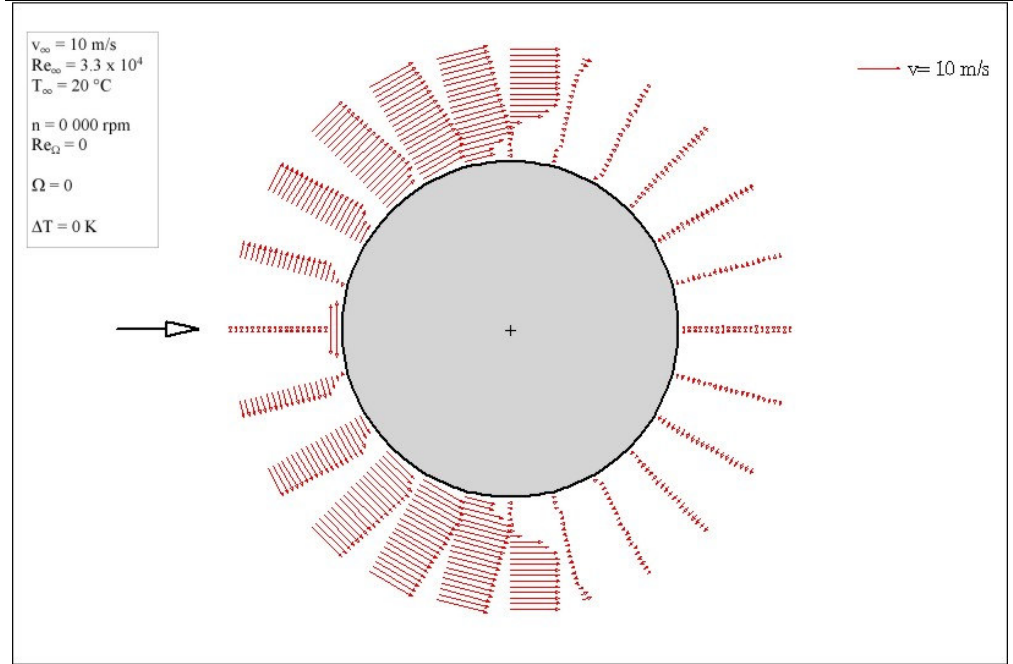
Figure 19

Figure 20

Figure 21

$v_\infty = 10$ m/s
$Re_\infty = 3.3$ x 10^4
$T_\infty = 20$ °C

$n = + 12\,000$ rpm
$Re_\Omega = 1.0$ x 10^5

$\Omega = 3.0$

$\Delta T = 0$ K

$v = 10$ m/s
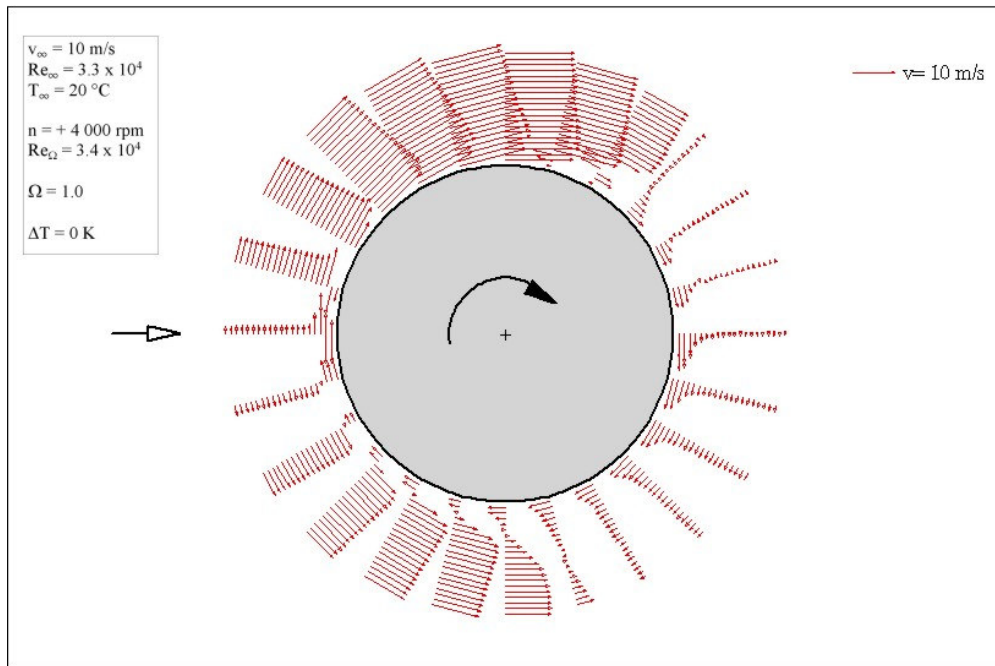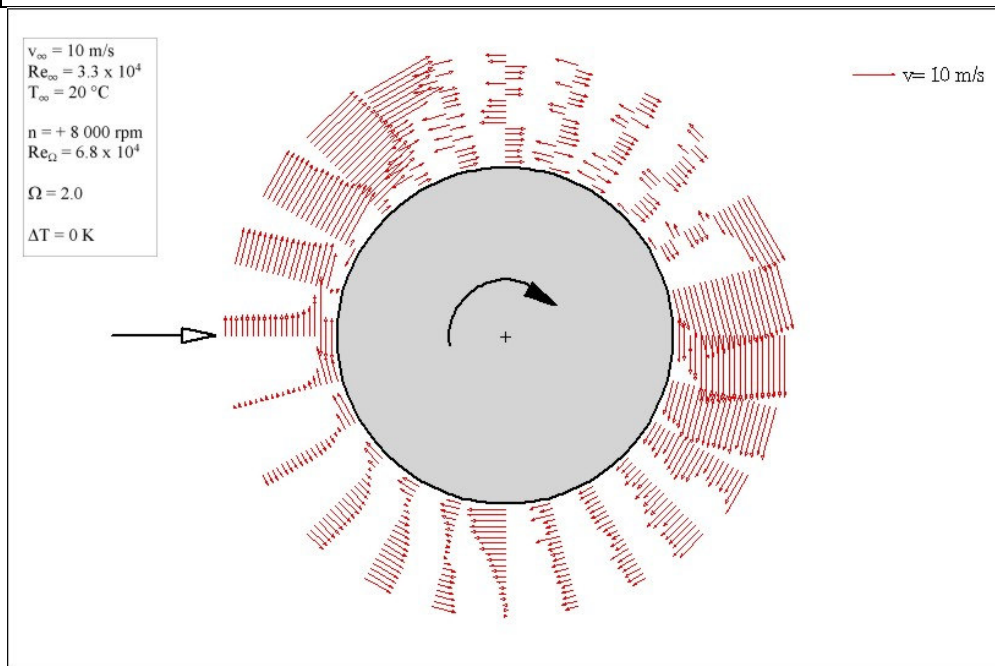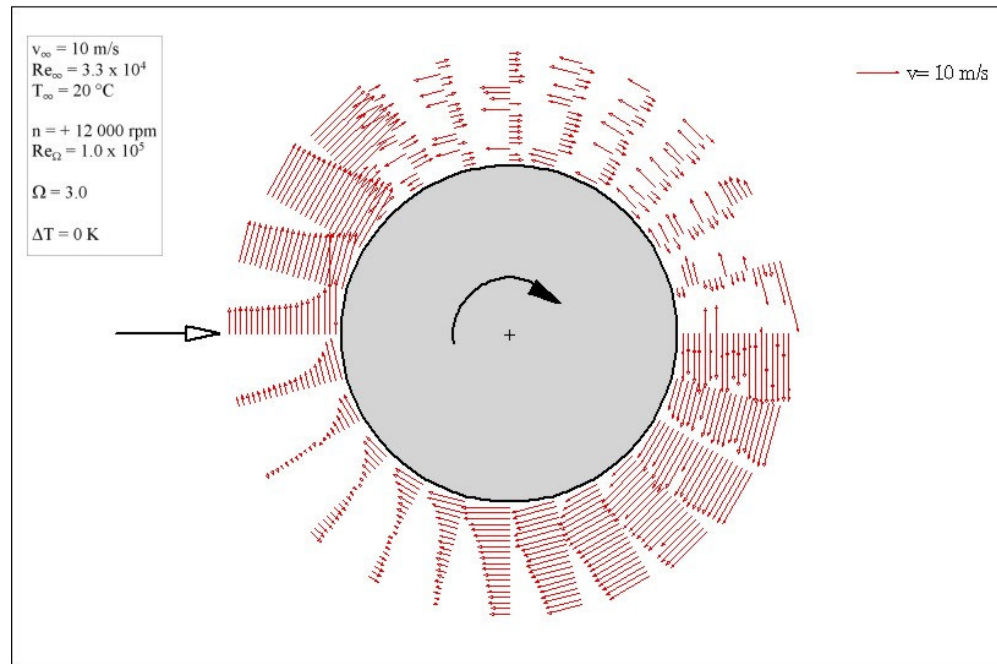
The influence of a heated wall on the velocity profile in the boundary layer is demonstrated in the following figures. Here, velocity profiles at the positions $\varphi = 30°$, $45°$ and $90°$ are given as examples. All experiments refer to a sub-critical flow at a Reynolds number $Re_\infty = 3.3$ x 10^4. In the case of the non-rotating cylinder (figure 22), a slight difference to the heated case (dotted lines) can be noticed up to a radial distance of 0.8 mm at $\varphi = 30°$ and $45°$. In both positions the local fluid velocities are higher at the heated wall. This can be explained by an increase in volume and thus an acceleration of the fluid due to the heat [20]. However, there is no difference near the separation point at $\varphi = 90°$. The small negative velocities in this area indicate the onset of recirculation, that is, the flow has already separated from the wall.

Figure 22
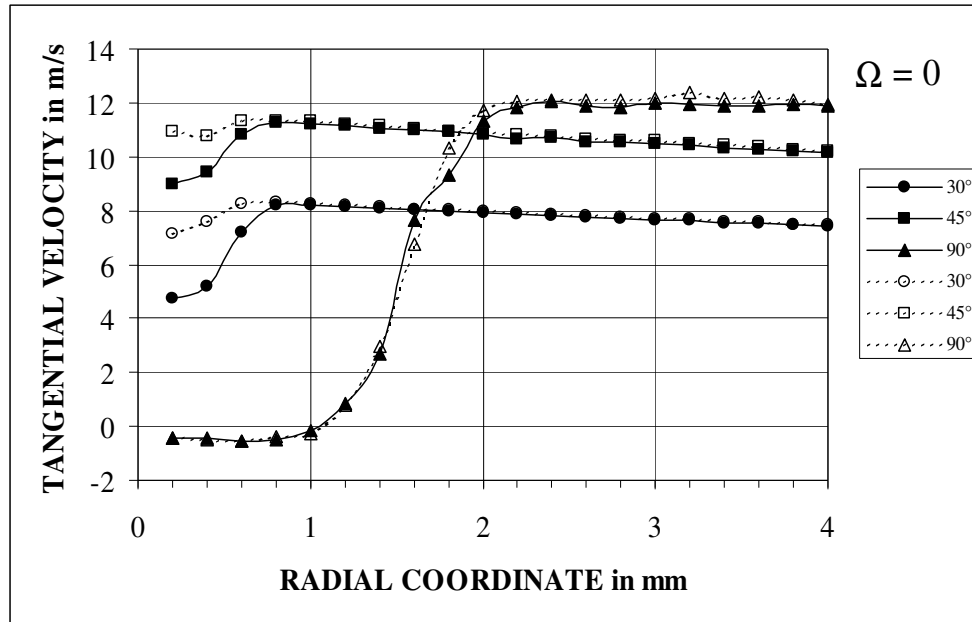
In figure 23 two positions of the rotating cylinder, both downstream (45° and 90°) and upstream (315° and 270°), are represented for the case of $\Omega = 1$. Here, exactly the opposite to the non-rotating cylinder can be observed, in that now the heated wall has a thicker boundary layer at $\varphi = 45°$ and 90°. On the opposite side, however, the situation is similar again to the non-rotating cylinder, if not as markedly.

In contrast to Oesterle [16] who could not observe differences between a heated and unheated wall in a sub-critical flow, these experiments clearly indicate a systematic influence of a heated wall on the velocity profiles in the boundary layer. Obviously, the relative velocity of the wall to the flow plays an important role in the effect of heat transfer on the behaviour of the laminar boundary layer. In the case of a relative movement, as it is the case at the non-rotating cylinder at $\varphi = 30°$ and 45° as well as at the rotating cylinder on the upstream side, the boundary layer appears to be thinner in the heated case. However, after the separation of the flow, a heated wall no longer has any impact at $\varphi = 90°$ as figure 22 illustrates. This confirms the well-known fact that a hot wall has a destabilising effect on the boundary layer of gases [20]. Peller [19] also made the observation, under comparable conditions, that the velocity boundary layer was thinner at a heated wall and he explains this by a change of viscosity at the respective fluid temperature.

27
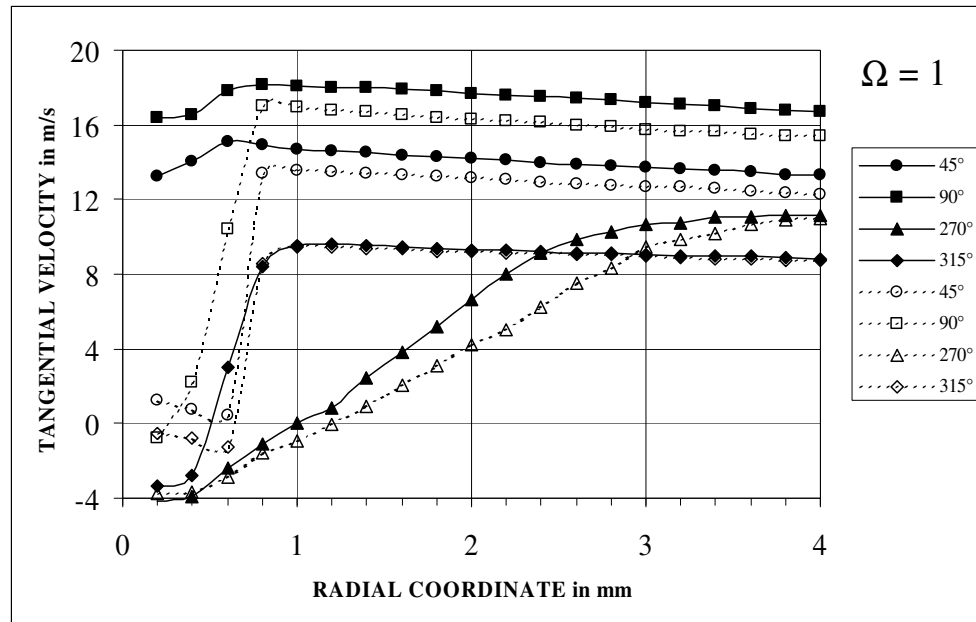
Figure 23

It should be noted that LDV-measurements are very difficult to perform at these close proximities to a wall and these reported results should be viewed with some caution. However, the good agreement of data points (such as at $\varphi = 90°$ in figure 22 and others) at distances as close as 0.2 mm from the wall, suggests that severe errors in other positions is unlikely.

Temperature gradients

As already mentioned, the beam of the laser which was used for the light-deflection had a diameter of only 0.3 mm but the fact that it was not infinitesimally small played an important role in the quantitative interpretation of the results. The exact conversion of the measured light-deflection to local Nusselt numbers could only happen if one knows which part of the boundary layer the light beam touches. Even more interesting than absolute figures of Nusselt numbers, however, is gaining an understanding of the influence of rotation and crossflow on local processes in the boundary layer. For this reason, the calculation of a Nusselt number was abandoned and instead the processes at the wall of the rotating cylinder were examined by the pure measured value "deflection". It is

28

important to note that, in any case, a high deflection means a high temperature gradient in the investigated area. Apart from that, reference measurements without heating but with rotation and crossflow show no effect of local pressure gradients on the light-deflection. This means that, in the following, the width of the thermal boundary layer is responsible for the deflection of the light-beam in the first place, whereas it is nearly identical with the velocity boundary layer in gases.

Figure 24
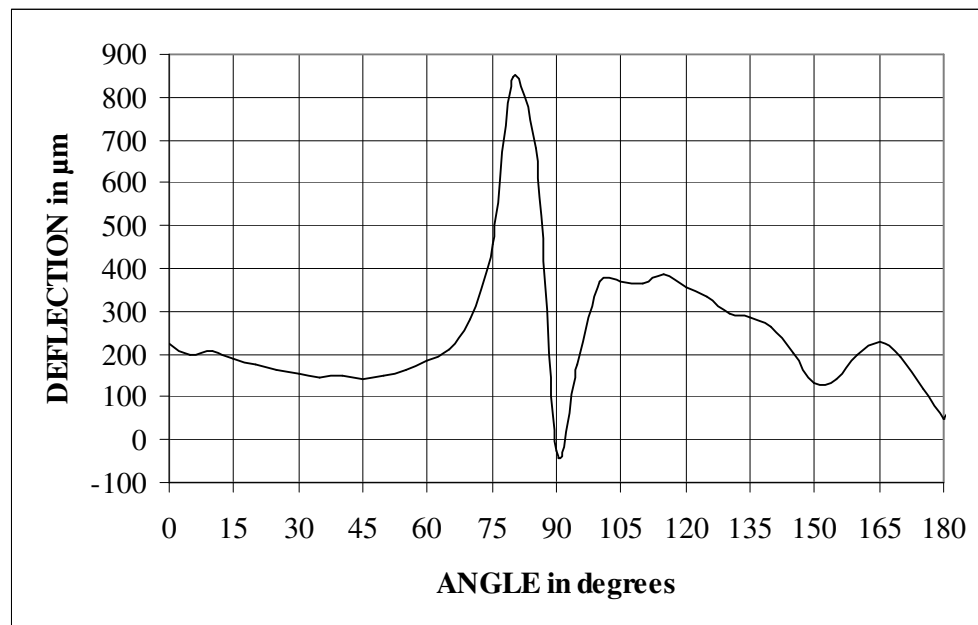
As an illustrative example, the measurement displayed in figure 24, the line of the light-deflection from the front stagnation point ($\varphi = 0°$) to the rear stagnation point ($\varphi = 180°$) at the non-rotating cylinder will be discussed. A laminar boundary layer begins to form downstream at the front stagnation point. The thinner it is, the smaller the thermal resistance and thus the greater the temperature gradient and the measured deflection. With increasing boundary layer thickness the light-deflection decreases. At about $\varphi = 45°$, a second effect comes to bear in this example. As soon as the boundary layer thickness reaches the diameter of the light-beam, the deflection starts to increase again. With the assumption that the temperature profile within the boundary layer always looks similar, regardless of the absolute thickness, this increase can be explained by the light-beam covering an area at the wall with an increasing temperature gradient. The boundary layer has reached its maximum thickness at about $\varphi = 80°$, where the measured

29

deflection shows a maximum. The dramatic drop of the deflection at $\varphi = 90°$ identifies the area where the boundary layer has already separated from the wall. Now, a turbulent area begins to form at the wall which increases the thermal resistance and results in a larger temperature gradient again. The consequence is a repeated increase of the measured light-deflection after the separation of the laminar boundary layer. However, the heat transfer is being improved by the turbulent flow further down the cylinder, which flattens the temperature gradient and thus the light-deflection. The local minimum at $\varphi = 150°$ may be explained by a separating vortex.
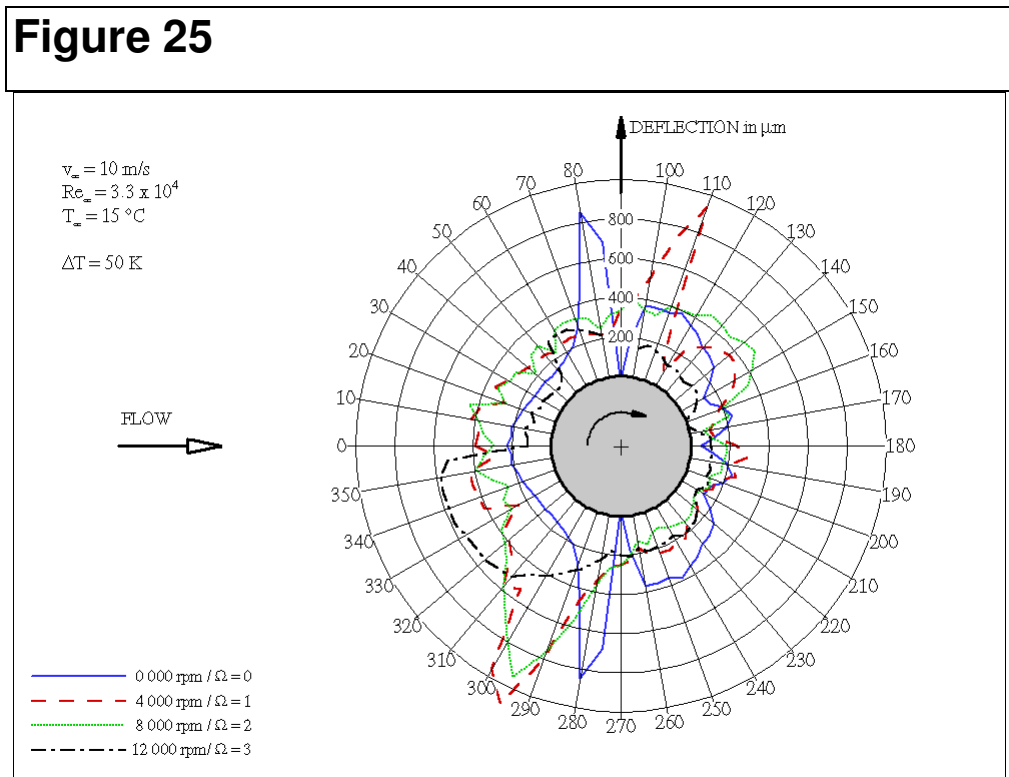
Figure 25

Only a few examples will be given here from the large number of experiments. Figure 25 shows a series of measurements at sub-critical flow at a Reynolds number $Re_\infty = 3.3 \times 10^4$, a temperature difference of 50 K and the rotational speed as a parameter. It can be seen that the downstream separation point (represented by the maximum at about $\varphi \approx 90°$) is shifted in rotational direction with increased speed. At about $\Omega = 2$ this point starts to disappear and the curve becomes flatter. The opposite separation point, however, is hardly shifted. Even at $\Omega = 3$ a maximum of light-deflection can still be observed, but not as marked as at lower speeds. Generally speaking, rotation seems to have an equalizing effect on the

shape of the graph as maxima and minima become less marked. Local, and for the heat transfer, characteristic points transit to a more and more uniform course.

The following pictures (figures 26 to 28) represent a series of outer field measurements in which the light-beam was moved up to a distance of 10 mm away from the wall. A three-dimensional view was chosen in order to give a better impression of what impact rotation has on thermal processes around the cylinder. Here, the position of the cylinder is marked in dotted lines and the view is oriented towards the downstream separation point. In the displayed relief, peaks represent points with the highest temperature gradient from the cylinder towards the fluid. The bizarre "ridges" thus identify the course of the separating flow from the cylinder.

Figure 26

$v_\infty = 10$ m/s
$Re_\infty = 3.3 \times 10^4$
$T_\infty = 15\ °C$

$n = 0\ 000$ rpm
$Re_\Omega = 0$

$\Omega = 0$

$\Delta T = 50$ K

FLOW

Figure 27

$v_\infty = 10$ m/s
$Re_\infty = 3.3 \times 10^4$
$T_\infty = 15\ °C$

$n = +\ 4\ 000$ rpm
$Re_\Omega = 3.4 \times 10^4$

$\Omega = 1.0$

$\Delta T = 50$ K

FLOW

Figure 28

$v_\infty = 10$ m/s
$Re_\infty = 3.3 \times 10^4$
$T_\infty = 15\ °C$

$n = +\ 8\ 000$ rpm
$Re_\Omega = 6.8 \times 10^4$

$\Omega = 2.0$

$\Delta T = 50$ K

FLOW
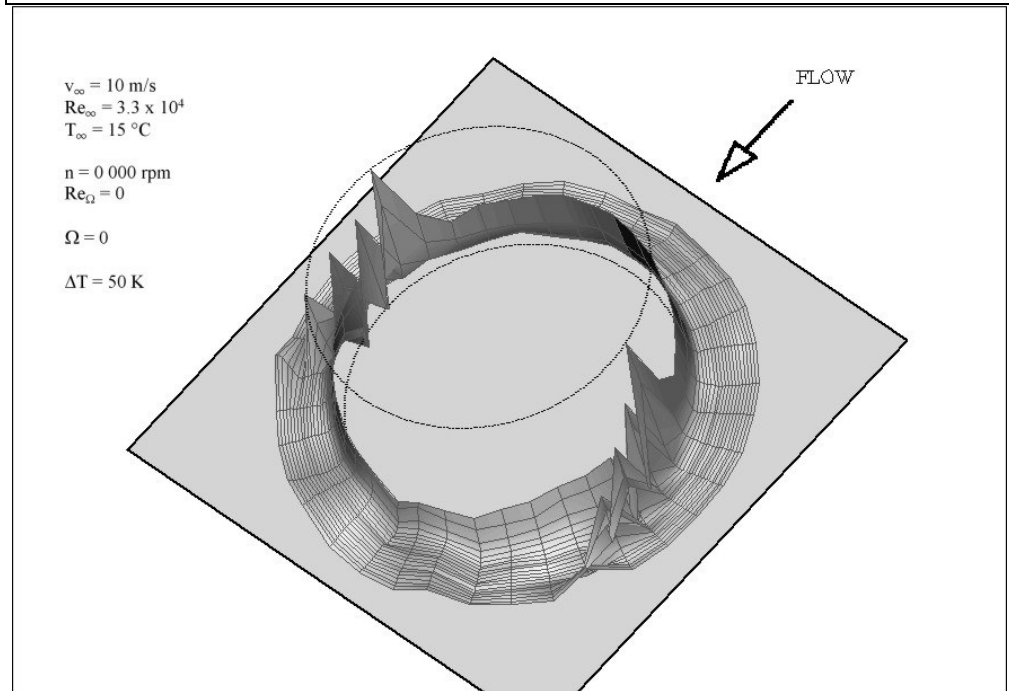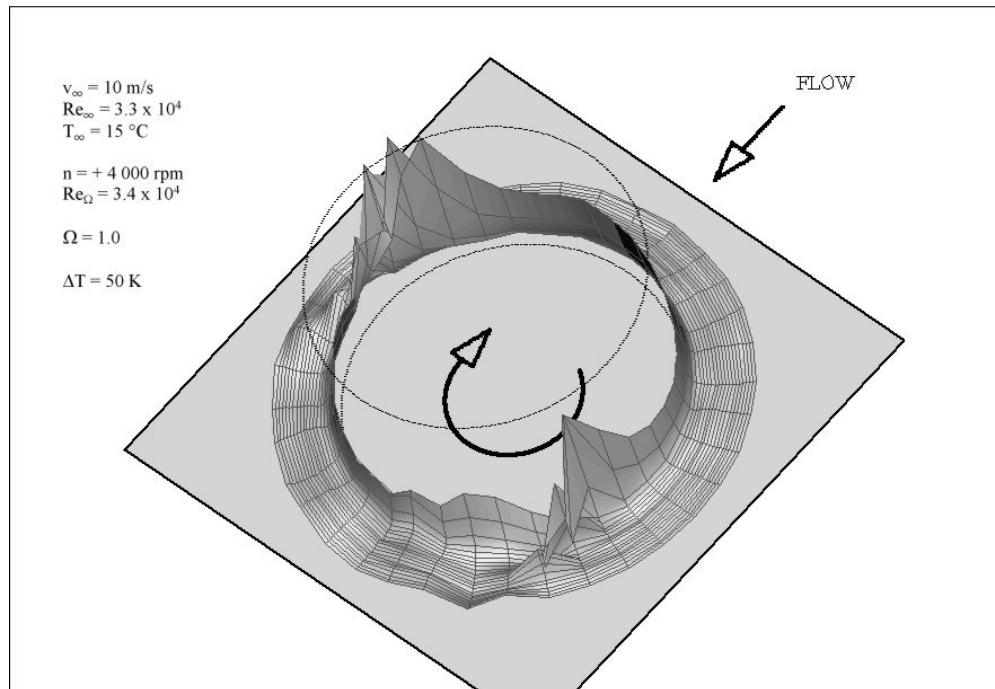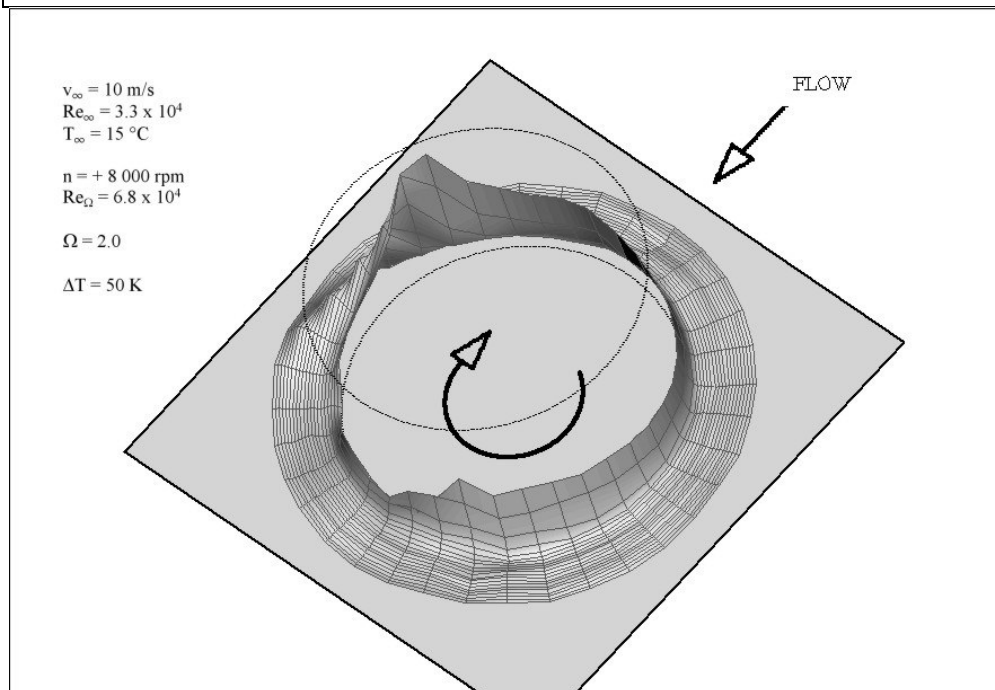
These measurements show quite clearly how the originally symmetrical relief at the non-rotating cylinder (figure 26) becomes distorted by rotation. Thus, the front separation point (in this view) is more shifted than the rear stagnation point at a velocity-ratio $\Omega = 1$ (figure 27). At $\Omega = 2$ (figure 28), however, the front

separation point has already dissolved, while the rear one is still visible, if less markedly. As well as the LDV-velocity-measurements, the experiments with the light-deflection-technique also show that the velocity ratio $\Omega = 2$ represents a very significant condition for the fluid flow and thermal processes near a rotating cylinder.

Temperature fields

The interferometer served the purpose of the qualitative assessment of the thermal processes at the rotating cylinder. In the following figures (figures 29 - 33) only the downstream half of the cylinder with its separation points and the turbulent wake is shown, as the high line-density in the upstream half (caused by the high temperature gradients there) was too high for the optical resolution. In each figure two quarter circles have been assembled to form one picture, the absolute symmetry in the case of the non-rotating cylinder arising from mirroring one photo. Flow- and rotational direction are marked by arrows. Since the vibrations caused by the fan and the electric motor had a bad influence on the quality of the produced interferograms, the experiments were carried out at low flow speeds of 1 to 2 m/s and rotational speeds of 800 to 1600 rpm. Even so, the expected processes are clearly evident.

Figure 29
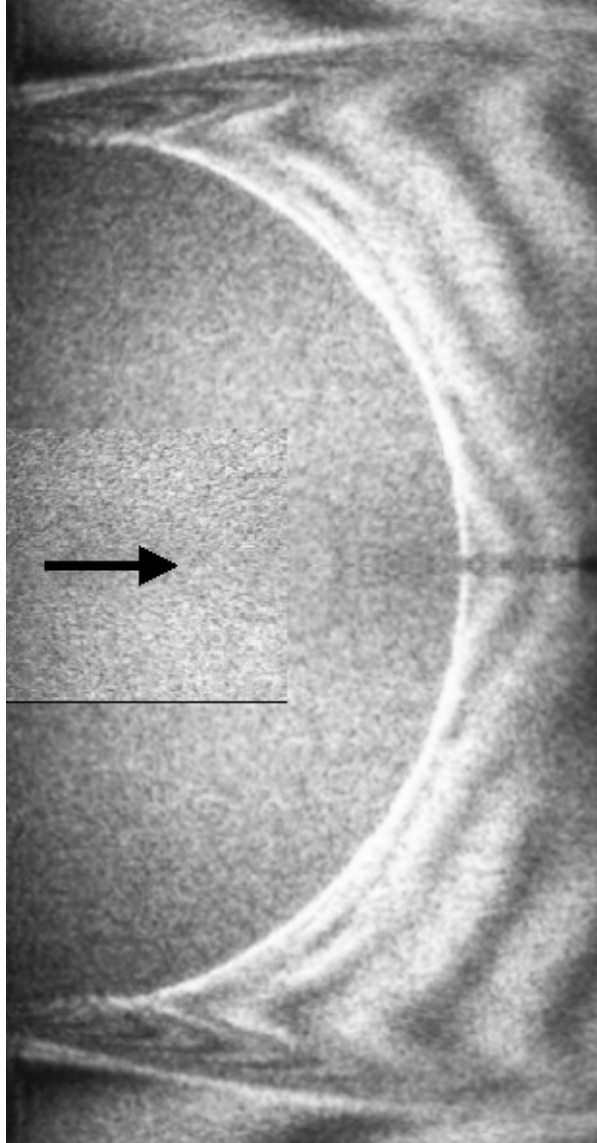
Figure 30
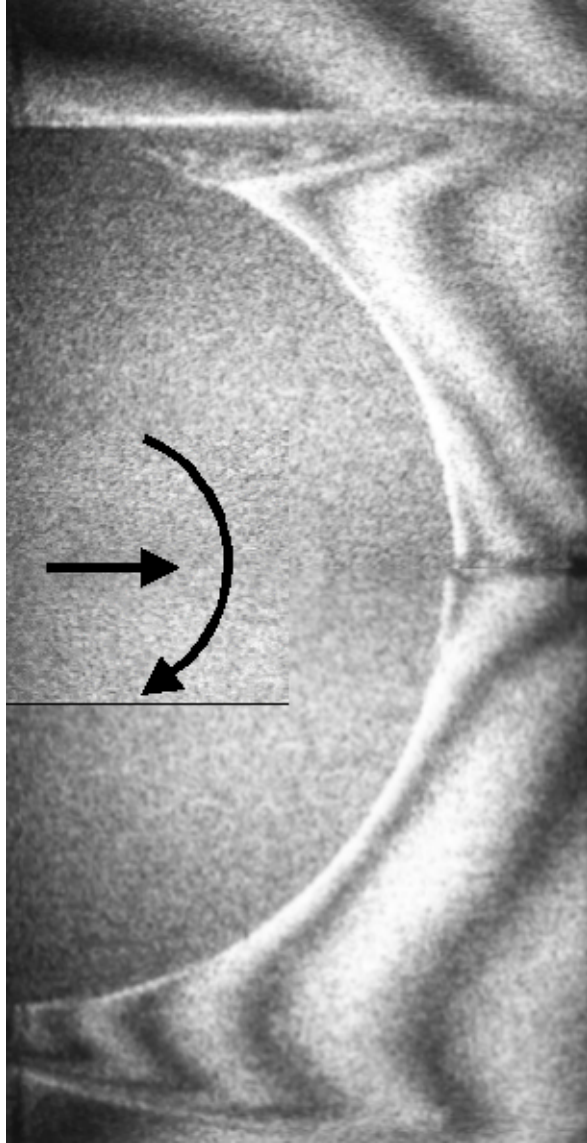
Figure 31
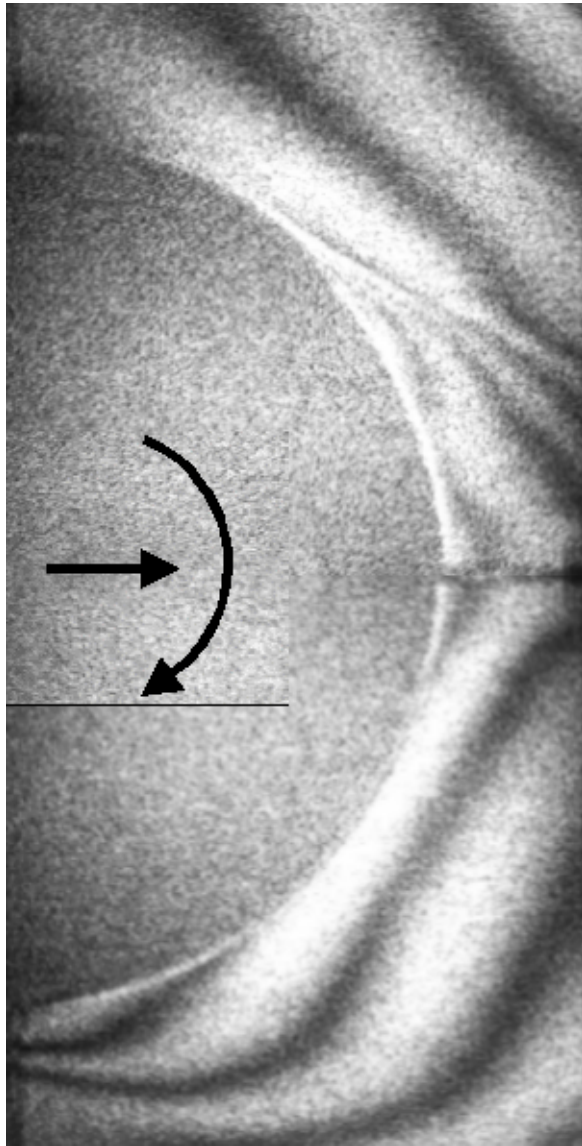
Figure 32
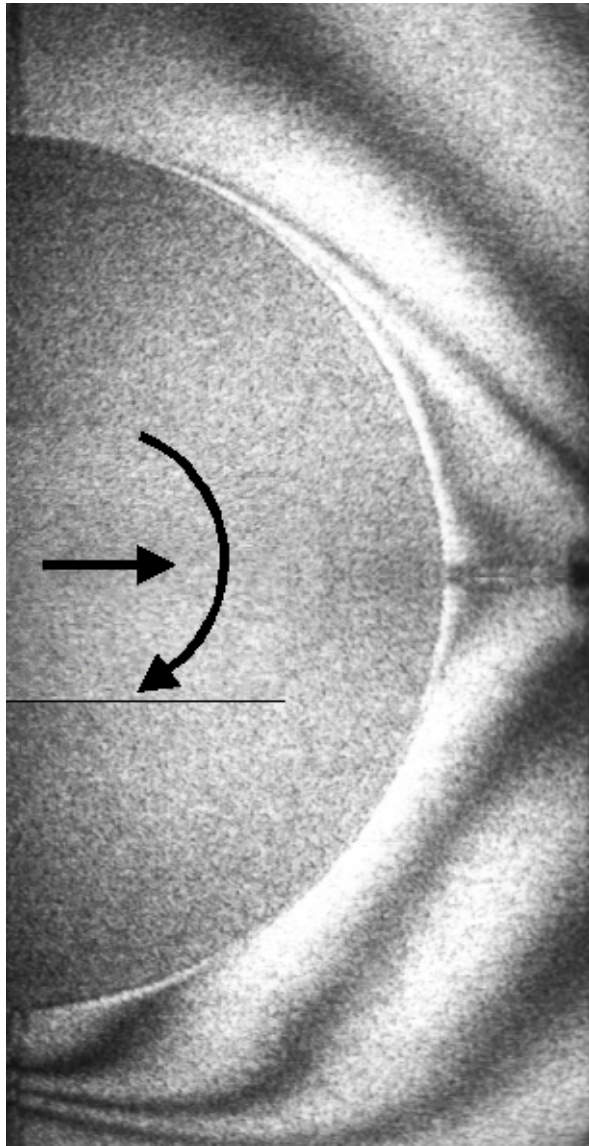
Figure 33
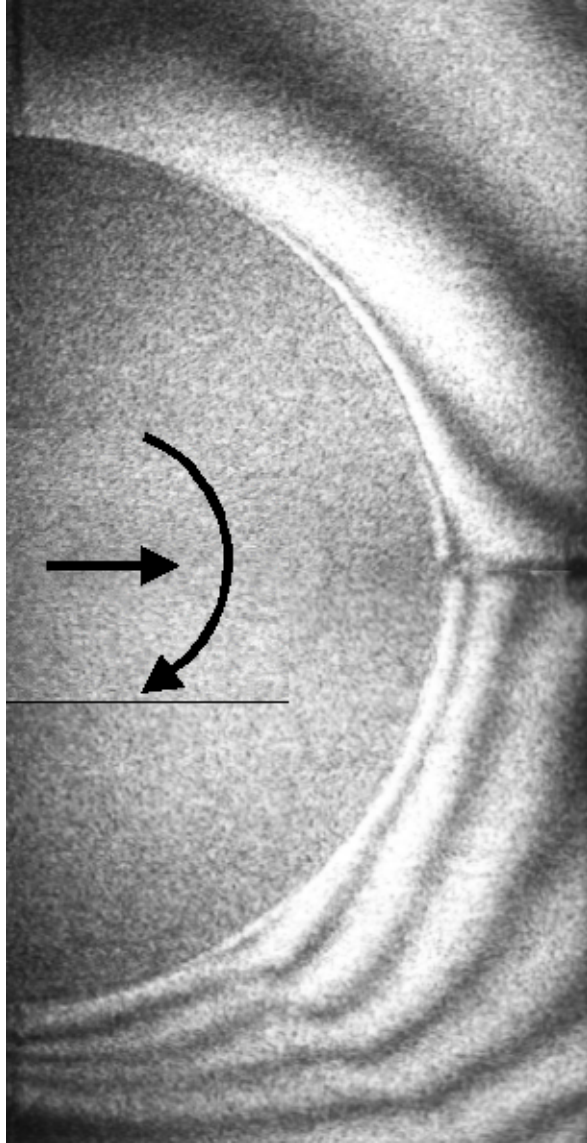
For instance, the velocity-ratio Ω behaved like an independent parameter, if the flow velocity was varied and rotational speed kept at a constant Ω. The non-rotating cylinder is represented in figure 29 at a Reynolds number $Re_\infty = 0.7 \times 10^4$. An area of densely crowded isothermals can be recognised, stretching from the separation point of the flow in tangential direction. The rotation of the cylinder results in a slight movement of the two separation points at $\Omega = 1$ (figure 30), whereas the downstream separation point seems to dissolve at $\Omega = 2$ (figure 31).

With reduced flow velocity, and rotational speed reduced proportionately in order to keep Ω constant, the same characteristics of the flow pattern remain. Figure 32 is the counterpart of figure 31 for $\Omega = 2$, but at half the flow velocity. A

comparison of both photographs makes plausible the assertion that Ω is an independent parameter, at least in this range of Reynolds numbers Re_∞. With further increased speed of the cylinder up to $\Omega = 3$ (figure 33), the downstream separation point has completely vanished. The displayed isothermal, in the form of a dark interference line, runs concentrically around the cylinder contour.

These interferometric pictures are strong confirmation of the results of the light-deflection experiments. The bent contour and the high density of the isothermal lines near the separation points at the cylinder wall represent the "integrated form" of the temperature gradients in the shape of "ridges" created by the light-deflection technique in figures 26 to 28.

Even more compelling than the shown interferometric photographs are moving pictures recorded by a video camera during the experiments. Those real-time pictures appear richer in contrast, as the human eye can identify dynamic changes better than can be detected from still pictures. Thus, the video recordings deliver a very vivid impression of the oscillating processes in the turbulent wake of the cylinder.

Conclusions

1. LDV-field-measurements of fluid velocities indicated a significant influence of rotation on the flow past a rotating cylinder, up to a distance of several cylinder diameters. The shift of the flow separation points due to rotation, the turbulent wake of the cylinder, and the existence of vortices in the wake could be identified clearly. However, a heated wall with a temperature difference of 50 K did not seem to change the flow pattern. The degree of turbulence of the flow in the wake of the cylinder was reduced significantly by rotation.

2. Velocity-measurements near the cylinder wall indicated an influence of a heated wall on the boundary layer thickness. It appears that the boundary layer is thinner in the heated case, as reported by various authors. Also, fluid velocities are higher near a heated wall, as expansion takes place due to the higher temperature.

3. A contact-free optical measurement technique was developed and verified to measure local temperature gradients in the boundary layer of a heated, rotating cylinder. An interpretation was given to verify the experimental results. Here, for instance, the local thermal boundary layer thickness could be determined and separation points could be identified.

4. Temperature gradient measurements with the light-deflection technique in the vicinity of the cylinder also detected similar thermal patterns, as flow patterns could be detected by LDV-measurements, such as flow separation and changes in the boundary layer thickness.

5. With a Michelson-interferometer, thermal fluctuations and the impact of rotation on heat transfer could be visualised. It seems that the velocity-ratio Ω behaves like an independent parameter, as flow and thermal patterns seem unchanged at various crossflow Reynolds numbers but constant velocity ratios. The interferograms also confirmed the results of the light-deflection technique and represented them in an integrated form.

Captions to figures

Figure 1:   View of the cylinder drive

Figure 2:   The components of the LDV-system

Figure 3:   The optical set-up of the light-deflection technique

Figure 4:   The qualitative deflection of the light beam in various sections of the boundary layer

Figure 5:   The measured light-deflection in radial direction. Here: Front stagnation point of the non-rotating cylinder at a crossflow of 10 m/s

Figure 6:   The experimental set-up of the Michelson-interferometer

Figure 7:   The flow around the non-rotating cylinder at $\Omega = 0$

Figure 8:   The streamlines at $\Omega = 0$

Figure 9:   The flow around the non-rotating cylinder at $\Omega = 1$

Figure 10:   The streamlines at $\Omega = 1$

Figure 11:   The flow around the non-rotating cylinder at $\Omega = 2$

Figure 12:   The streamlines at $\Omega = 2$

Figure 13:   The flow around the non-rotating cylinder at $\Omega = 3$

Figure 14:   The streamlines at $\Omega = 3$

Figure 15:   The degree of turbulence in the wake of the non-rotating cylinder

References

1. Reid E G: Tests of rotating cylinders. NACA TN 209 (1924)

2. Thom A: Experiments on the air forces on rotating cylinders. ARC R and M 1018 (1925)

3. Thom A: The pressures round a cylinder rotating in an air current. ARC R and M 1082 (1926)

4. Thom A: Experiments on the flow past a rotating cylinder. ARC R and M 1410 (1931)

5. Prandtl L: Magnuseffekt und Windkraftschiff. Naturwissenschaften 13. Jg. (1925) 93 – 108

6. Swanson W M: The Magnus effect: A summary of investigations to date. J. Basic Engineering 83 (1961) 461 – 470

7. Anderson J T, Saunders O A: Convection from an isolated heated cylinder rotating about its axis. Proceedings of the Royal Society of London, England, Series A, Vol. 217 (1953) 555

8. Etemad G A: Free-convection heat transfer from a rotating horizontal cylinder to ambient air with interferometric study of flow. Trans. Amer. Soc. Mech. Eng. 77 (1955) 1283

9. Dropkin D, Carmi A: Natural-convection heat transfer from a horizontal cylinder rotating in air. Trans. Amer. Soc. Mech. Eng. 79 (1957) 741

10. Kays W M, Bjorklund J S: Heat transfer from a rotating cylinder with and without crossflow. Trans. ASME 80 C (1958) 70 –78

11. Yildiz A : Zum Wärmeübergang am Kommutator. Dissertation, T.U. Berlin 1964

12. Geropp D: Der turbulente Wärmeübergang am rotierenden Zylinder. Ingenieur Archiv 38 (1969) 195 – 203

13. Gschwendtner M A: The Eckert number phenomenon. Heat & Mass Transfer (2003)

14. Peller H, Lippig V, Straub D, Waibel R: Thermofluiddynamic experiments with a heated and rotating circular cylinder in crossflow, part 1: Sub-critical heat transfer measurements. Experiments in Fluids 2 (1984) 113 – 120

15. Badr H M, Dennis S C R: Laminar forced convection from a rotating cylinder. Int. J. Heat Mass Transfer Vol. 28 No. 1 (1985) 253 – 264

16. Oesterle M: Zur Topologie der Feld- und Grenzschichtstrukturen beim Wärmeübergang am querangeströmten, beheizten und rotierenden Zylinder. Experimentelle Untersuchungen für Fluide unterschiedlicher Prandtl-Zahl. Fortschr.-Ber. VDI Reihe 7 Nr. 299 Düsseldorf VDI Verlag 1996

17. Wurst T, Oesterle M, Straub D: Windkanal für Wärmeübergangsmessungen. Zeitschrift für Versuchs- und Forschungsingenieure 6 (1991) 27 – 29

18. Schmidt E: Schlierenaufnahmen des Temperaturfeldes in der Nähe wärmeabgebender Körper. Forschg. Ing.-Wes. Bd. 3, Heft 4 (1932) 181 – 189

19. Peller H: Thermofluiddynamic experiments with a heated and rotating circular cylinder in crossflow, part 2.1: Boundary layer profiles and location of separation points. Experiments in Fluids 4 (1986) 223 – 231

20. Schlichting H, Gersten K: Grenzschicht-Theorie. Springer-Verlag, Berlin, Heidelberg (1997) 9. Aufl.

Acknowledgements